CHALMERS
UNIVERSITY OF TECHNOLOGY

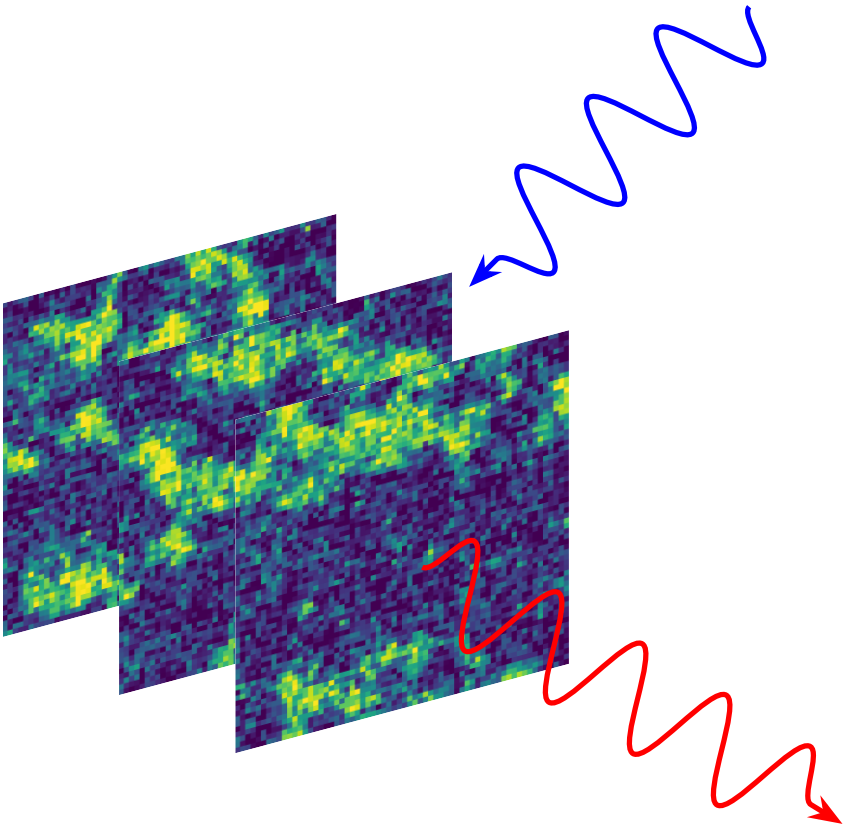

Entropy Production of a Harmonically Driven Order Parameter Field

A Field Theoretic Approach to Ultrafast Thermodynamics

Master's thesis in Physics

ERIK KARLSSON ÖHMAN

DEPARTMENT OF PHYSICS
CHALMERS UNIVERSITY OF TECHNOLOGY
Gothenburg, Sweden 2025
www.chalmers.se

Master's thesis 2025

Entropy Production of a Harmonically Driven Order Parameter Field

A Field Theoretic Approach to Ultrafast Thermodynamics

ERIK KARLSSON ÖHMAN

CHALMERS
UNIVERSITY OF TECHNOLOGY

Department of Physics
Division of Condensed Matter and Materials Theory
Geilhufe group
Chalmers University of Technology
Gothenburg, Sweden 2025

Entropy Production of a Harmonically Driven Order Parameter Field
A Field Theoretic Approach to Ultrafast Thermodynamics
ERIK KARLSSON ÖHMAN

Supervisor: Dr. R. Matthias Geilhufe, Department of Physics
Examiner: Dr. R. Matthias Geilhufe, Department of Physics

Master's Thesis 2025
Department of Physics
Division of Condensed Matter and Materials Theory
Geilhufe group
Chalmers University of Technology
SE-412 96 Gothenburg
Telephone +46 31 772 1000

Cover: Illustrative sketch showing the time evolution of a harmonically driven scalar order parameter field. The blue arrow represents the external driving field, while the arrow in red represents the corresponding entropy production.

Typeset in LaTeX
Printed by Chalmers Reproservice
Gothenburg, Sweden 2025

Entropy Production of a Harmonically Driven Order Parameter Field
A Field Theoretic Approach to Ultrafast Thermodynamics
ERIK KARLSSON ÖHMAN
Department of Physics
Chalmers University of Technology

Abstract

Ultrafast thermodynamics is an emerging field of research that aims to model the non-equilibrium dynamics of laser-excited materials. A central quantity of interest is the entropy production, which quantifies how far a system is from equilibrium. While previous theoretical works have modeled the entropy production in terms of lattice vibrations and magnetization dynamics, this work models the entropy production of a scalar order parameter field coupled to a time-dependent harmonic driving field. In doing so, this thesis takes the first steps in bridging the gap between ultrafast thermodynamics and statistical field theory.

The evolution of the field is modeled by the time-dependent Ginzburg-Landau equation, which is solved numerically. In the absence of a driving field, the validity of this method is confirmed through a finite-size scaling analysis in which equilibrium critical exponents are extracted and shown to agree with known values of the Ising/ϕ^4 universality class.

An analytical expression for the entropy production is also proposed. This expression is compared with numerical simulations and, for a selected range of driving frequencies, exhibits clear quantitative agreement in the high-temperature phase. A finite-size scaling analysis of the entropy production further suggests that, for the driving protocol in question, the entropy production converges to a smooth function around the critical temperature, and as such does not exhibit any critical scaling.

Keywords: Entropy production, criticality, time-dependent Ginzburg-Landau equation, ultrafast thermodynamics

Acknowledgements

I would like to express my gratitude to Dr. R. Matthias Geilhufe for supervising and examining this thesis. Your guidance and advice have been much appreciated. A big thanks also goes to Jacob Ljungberg for acting as the opponent and for proofreading the thesis. Finally, I would like to thank my friends and family for their support during the writing of this thesis and throughout my studies.

Erik Karlsson Öhman, Gothenburg, June 2025

Contents

List of Figures

List of Tables

1
Introduction

This chapter provides the background motivating this field of inquiry. Moreover, the aim of this thesis along with relevant delimitations is presented, followed by an overview of the thesis structure.

1.1 Background

Ultrafast spectroscopy is a field that aims to study the non-equilibrium behavior of materials by exciting them with laser pulses, typically in the terahertz frequency range. In recent years, the field has progressed significantly. New experimental methods and technologies – such as high-harmonic generation (HHG), chirped pulse amplification (CPA) and Ti:sapphire lasers, to name a few [1] – have enabled physicists to probe materials on unprecedentedly short timescales, ranging from picoseconds down to attoseconds [2]. This has enabled the realization and investigation of photo-induced phenomena such as high-temperature superconductivity in organic compounds [3], the anomalous Hall effect in graphene [4] and ultrafast switching of magnetization [5]. Most importantly, these are properties that are not exhibited in equilibrium and they are in many cases driven by mechanisms that cannot solely be explained with a thermal description of the system in question – in other words: some mechanism beyond heating is at play [6].

A key quantity to understanding non-equilibrium phenomena is *entropy production*. The concept of entropy production is one of the cornerstones of *stochastic thermodynamics* – a relatively new field that extends traditional thermodynamics into the non-equilibrium microscopic regime, by assigning entropy to individual fluctuating trajectories. Originally conceived of to study active matter such as colloidal particles and single biomolecules [7], the framework of stochastic thermodynamics has also proven to be a useful tool in modeling entropy production in ultrafast spectroscopy experiments. This emergent branch of research is aptly known as *ultrafast thermodynamics* [8, 9].

Since entropy production is related to heat dissipated through irreversible processes in a system, modeling of entropy production could be of great practical importance in the future design of electronics that rely on ultrafast light-matter interaction, such as THz spintronics and all-optical switches [10]. On a deeper level, however, the entropy production rate is innately connected to how non-

equilibrium systems evolve [11] and it provides a quantitative measure of to what extent a system is out of equilibrium [12].

Previous theoretical studies on ultrafast thermodynamics have modelled the stochastic dynamics of materials in terms of collective excitations, such as lattice vibrations [8] and magnetization dynamics [9]. Notwithstanding the success of these models, this picture is inherently limited – it cannot accurately describe critical phenomena such as phase transitions. This work seeks to move beyond that limitation by calculating the entropy production of a scalar order parameter field. In doing so, it takes the first steps towards formulating a field-theoretic framework for ultrafast thermodynamics and understanding the critical behavior of ultrafast entropy production.

1.2 Aim

This thesis aims to assert the validity of the time-dependent Ginzburg-Landau model for simulating the critical phenomena of the Ising/ϕ^4 universality class. This will be done by extracting the static critical exponents of some relevant thermodynamic quantities through numerical finite-size scaling simulations. Furthermore, previous work on ultrafast entropy production will be extended to now encompass a field-based formalism. As such, an expression for the entropy production of a scalar order parameter field coupled to an external time-dependent magnetic field will be derived. This expression, in combination with numerical time-dependent Ginzburg-Landau simulations, will be used to investigate the temperature dependence of the entropy production in the vicinity of the field's critical temperature, T_C.

1.2.1 Delimitations

This thesis will only focus on classical physics, and as such will not treat the rich theory of quantum phase transitions. Moreover, the external fields investigated in this thesis are restricted to periodic, spatially homogeneous sinusoidal fields. This choice of field will be further motivated in Section 3.2.2.

1.3 Structure

Chapter 2 covers the theoretical background needed to approach the contents of this thesis, starting with a brief introduction to critical phenomena, followed by sections on finite-size scaling theory, time-dependent Ginzburg-Landau theory and stochastic thermodynamics.

Chapter 3 outlines the methods used for the numerical simulations.

Chapter 4 presents results and interpretations of numerical simulations, pertaining both to equilibrium and non-equilibrium phenomena.

Chapter 5 summarizes the conclusions drawn from this work, and details possible future research directions building on this work.

2
Theory

In this chapter, the theoretical underpinnings of this thesis are presented. Critical phenomena are introduced and motivated through the mean-field Ising model. This description is then further generalized to admit the study of critical exponents, universality classes, and finite-size scaling. Furthermore, the time-dependent Ginzburg-Landau equation is introduced, and it is made clear how it can be used in the framework of stochastic thermodynamics to compute quantities such as entropy production.

2.1 Phase Transitions and Critical Phenomena

Its a peaceful Wednesday morning in May. You wake to the sound of birds chirping and a gentle beam of sunlight hitting your face. After getting out of bed, you step into the bathroom for a warm shower. As you towel off, you notice the mirror fogging up. In the kitchen, you put a kettle on the stove and crack an egg into a hot frying pan.

Phase transitions might at first seem deceptively mundane – we are surrounded by them all the time. In fact, during this hypothetical May morning, you have already encountered three: condensation on the mirror, boiling water for your tea, and the denaturation of proteins as the egg cooks. Despite this, we will soon see that the concept of phase transitions – and the closely related notion of critical phenomena, possess an immense theoretical depth, which can give us profound insights into the laws governing our universe.

Generally speaking, a phase transition is the process of some system transitioning from one distinct state to another. Associated with a phase transition is an *order parameter* – some quantity of the system that unambiguously characterizes which phase the system is in.

In statistical physics, the Ising model is ubiquitous in its role of describing phase transitions. The model was originally conceived of to describe ferromagnetism, but has since found applications across a wide range of fields, including epidemiology [13], traffic flow modelling [14] and social science [15], to name a few. The system of interest in the Ising model consists of discrete magnetic moments, s_i, that can take one of two values, $s_i = \{-1, 1\}$. These magnetic moments, or spins, are, as illustrated in Figure 2.1, situated on a d-dimensional lattice and the

resulting Hamiltonian of the system is given by

$$H_{\text{Ising}} = -\sum_{ij} J_{ij} s_i s_j - h \sum_{i}^{N} s_i, \tag{2.1}$$

where J_{ij} is some correlation matrix that describes the interaction of the spins and h is an external magnetic field. Despite its innocuous appearance, this Hamiltonian can become, due to the interaction of spins, notoriously hard to compute exactly.

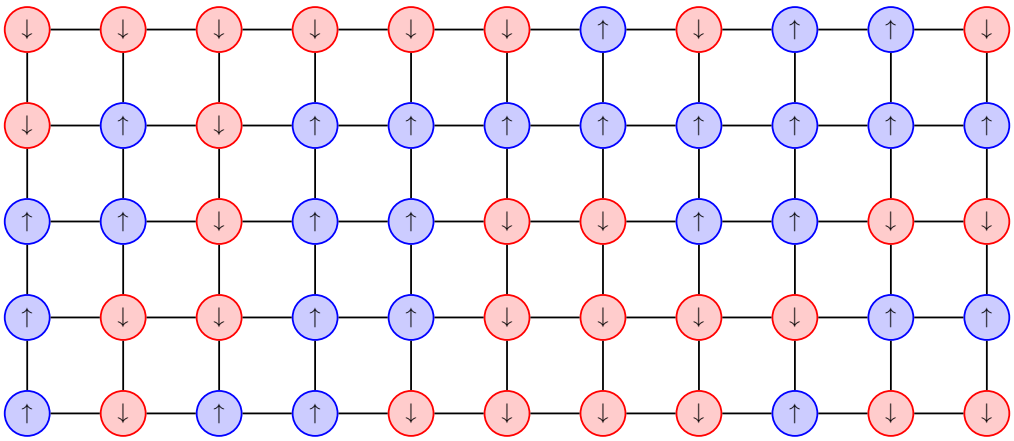

Figure 2.1: A 2D Ising model, consisting of magnetic moments on a lattice that either point upwards or downwards.

Solutions exist; in 1925 Ernst Ising solved it for a one dimensional chain with only nearest-neighbor interactions between spins [16], and in 1944 Lars Onsager famously proposed his solution for a two dimensional infinite lattice with no external field, also restricting himself to nearest neighbor interactions [17]. For three dimensions however, an analytical solution has yet to be discovered [18]. However, we will now see that by making simplifying assumptions we can arrive at a very elegant and general solution of the Ising model.

2.1.1 Mean-field Approximation

Let us start by revisiting the Ising Hamiltonian

$$H_{\text{Ising}} = -\sum_{ij} J_{ij} s_i s_j - h \sum_{i=1}^{N} s_i. \tag{2.2}$$

To make this problem more tractable we will make the correlation matrix J_{ij} explicit and assume that it encodes only nearest-neighbor interactions. As such,

we can now rewrite the correlation matrix in the Hamiltonian as

$$-\sum_{ij} J_{ij} s_i s_j \to -J \sum_{\langle ij \rangle} s_i s_j, \tag{2.3}$$

where we let $\langle ij \rangle$ denote summation over nearest neighbors and we assume $J > 0$. We will now introduce an order parameter

$$m \equiv \frac{1}{N} \sum_{i=1}^{N} \langle s_i \rangle, \tag{2.4}$$

where the expectation value is formally defined as

$$\langle s_i \rangle = \frac{\mathrm{Tr}(s_i e^{-\beta H_{\mathrm{Ising}}})}{\mathcal{Z}} \tag{2.5}$$

and $\mathcal{Z} = \mathrm{Tr}(e^{-\beta H_{\mathrm{Ising}}})$ denotes the canonical partition function. In the physical context of magnetism, we may interpret the order parameter, m, as the *magnetization* of our system. Moreover, when $m = 0$, our system is completely disordered or in other words: *paramagnetic*. Conversely, when $m \neq 0$, our system possesses some amount of order and is thus *ferromagnetic*. To proceed analytically, we will perform a key simplifying assumption. We assume that thermal fluctuations are small and proceed to define the fluctuation of the spins as

$$\delta s_i \equiv s_i - \langle s_i \rangle, \tag{2.6}$$

i.e. the deviation from the mean spin. Consequently, we may now express the spin-spin interaction term as

$$s_i s_j = (\delta s_i + \langle s_i \rangle)\left(\delta s_j + \langle s_j \rangle\right) = \langle s_i \rangle \langle s_j \rangle + \langle s_i \rangle \delta s_j + \langle s_j \rangle \delta s_i + \cancelto{0}{\delta s_i \delta s_j}. \tag{2.7}$$

where we set the term quadratic in fluctuations to zero, since the fluctuations of the spins were assumed to be small. This is known as the *mean-field approximation* and using it will simplify our calculations considerably. Now we can write the spin-spin interaction term as

$$s_i s_j \approx s_i \langle s_j \rangle + s_j \langle s_i \rangle - \langle s_i \rangle \langle s_j \rangle. \tag{2.8}$$

Moreover, since the Ising Hamiltonian is translationally invariant we may set $m = \langle s_i \rangle$. Consequently, the mean-field Ising Hamiltonian becomes

$$H_{\mathrm{MF}} = -Jm \sum_{\langle ij \rangle} \left(s_i + s_j - m\right) - h \sum_{i=1}^{N} s_i. \tag{2.9}$$

We may rewrite the sum over nearest neighbors further,

$$\sum_{\langle ij \rangle} (s_i + s_j) = \frac{q}{2} \sum_{i=1}^{N} 2 s_i, \tag{2.10}$$

where q denotes the number of neighbors for each lattice site. At last, we arrive at

$$H_{MF} = -\frac{qJm}{2} \sum_{i=1}^{N} (2 s_i - m) - h \sum_{i=1}^{N} s_i = \frac{NqJm^2}{2} - h_{\mathrm{eff}} \sum_{i=1}^{N} s_i, \tag{2.11}$$

where $h_{\mathrm{eff}} \equiv h + qJm$.

2.1.2 Thermodynamic Properties

Let us now revisit the partition function with the mean field Hamiltonian

$$\begin{aligned}\mathcal{Z}_{\mathrm{MF}} &= \prod_{i=1}^{N}\left(\sum_{s_i=\pm 1} e^{-\beta H_{MF}}\right) = e^{-\beta N q J m^2/2}\prod_{i=1}^{N}\left(e^{\beta h_{\mathrm{eff}}}+e^{-\beta h_{\mathrm{eff}}}\right) \\ &= e^{-\beta N q J m^2/2}\left(2\cosh \beta h_{\mathrm{eff}}\right)^N .\end{aligned} \tag{2.12}$$

Having calculated the partition function we may now express the order parameter as

$$m = \frac{1}{N}\sum_{i=1}^{N}\frac{\mathrm{Tr}(s_i e^{-\beta H_{\mathrm{MF}}})}{\mathcal{Z}_{\mathrm{MF}}} = \frac{1}{N}\frac{1}{\mathcal{Z}_{\mathrm{MF}}}\mathrm{Tr}\left(\sum_{i=1}^{N} s_i e^{-\beta H_{\mathrm{MF}}}\right), \tag{2.13}$$

where we exploited the additivity of the trace in the last step. To proceed we note that the derivate of the partition function with respect to the effective field is equal to

$$\frac{\partial \mathcal{Z}_{\mathrm{MF}}}{\partial h_{\mathrm{eff}}} = \beta\sum_{i}^{N}\mathrm{Tr}\left(s_i e^{-\beta H_{\mathrm{MF}}}\right). \tag{2.14}$$

Combining Equation (2.12), Equation (2.13) and Equation (2.14) thus gives us

$$m = \frac{1}{\beta N}\frac{1}{\mathcal{Z}_{\mathrm{MF}}}\frac{\partial \mathcal{Z}_{\mathrm{MF}}}{\partial h_{\mathrm{eff}}} = \frac{1}{\beta N}\frac{\partial \ln \mathcal{Z}_{\mathrm{MF}}}{\partial h_{\mathrm{eff}}} = \tanh\left(\beta h_{\mathrm{eff}}\right). \tag{2.15}$$

Recalling the definition of the effective field, we are finally left with

$$m = \tanh\left(\beta\left(h + qJm\right)\right). \tag{2.16}$$

This equation lacks an analytical solution but may be solved numerically. In Figure 2.2 we see that the magnetization decays rapidly as we approach $1/\beta qJ = 1$ from below. We may also note that, since tanh is an odd function, Equation (2.16) admits both a negative and positive solution. Both solutions are physically meaningful and correspond to the two directions of magnetization of a ferromagnet. The lowest temperature for which Equation (2.16) is solved by $m = 0$ is called the *critical temperature*:

$$T_C \equiv \frac{Jq}{k_B}, \tag{2.17}$$

and it is the temperature where the system transitions from the ferromagnetic phase to the paramagnetic phase. What really interests us is how the order parameter (and other thermodynamic quantities) behave in the vicinity of this temperature. As such we will Taylor expand Equation (2.16) at $T \sim T_C$, where m is small,

$$m \approx \frac{T_C}{T}m + \beta h - \frac{1}{3}\left(\frac{T_C}{T}\right)^3 m^3, \tag{2.18}$$

where we only kept the leading order term in h. Solving for $h \to 0$ we get

$$m = \begin{cases} \pm\sqrt{3\left(\frac{T}{T_C}\right)^2\left(\frac{T_C - T}{T_C}\right)} & T < T_C \\ 0 & T > T_C \end{cases}, \tag{2.19}$$

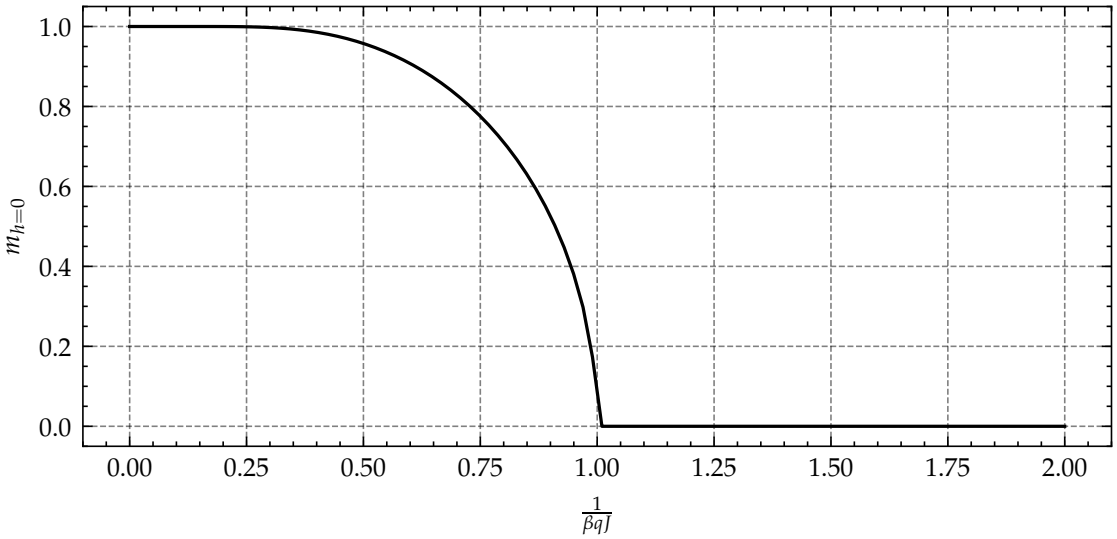

Figure 2.2: Numerical, positive solution of Equation (2.16) for $h = 0$. When $\frac{1}{\beta q J} = 1$ the system crosses over from being having a non-zero magnetism to being paramagnetic.

and for small $|T - T_C|$ and when approaching T_C from below, we can say that the magnetization behaves like

$$m \sim |T_C - T|^{\beta}, \tag{2.20}$$

where $\beta = \frac{1}{2}$, is a so-called *critical exponent*. At the moment this result may not look terribly interesting, but we will soon learn that studying the critical exponents associated with a phase transition actually can give us profound insights into the universal behavior shared by seemingly unrelated physical systems. First, however, we will see that many other thermodynamic quantities also follow a power law behavior near the critical temperature. Let us start by looking at the zero external-field magnetic susceptibility,

$$\chi = \left.\frac{\partial m}{\partial h}\right|_{h \to 0}. \tag{2.21}$$

Differentiating both sides of Equation (2.18) with respect to h yields

$$\chi \approx \frac{T_C}{T}\chi + \beta - \left(\frac{T_C}{T}\right)^3 m^2 \chi, \tag{2.22}$$

and after rearranging we get

$$\chi = \frac{\beta}{1 - \frac{T_C}{T} + \left(\frac{T_C}{T}\right)^3 m^2}. \tag{2.23}$$

Using the expression for m from Equation (2.19), we finally get

$$\chi = \begin{cases} 1/(k_B(T - T_C)) & T > T_C \\ 1/(2k_B(T_C - T)) & T < T_C \end{cases}. \tag{2.24}$$

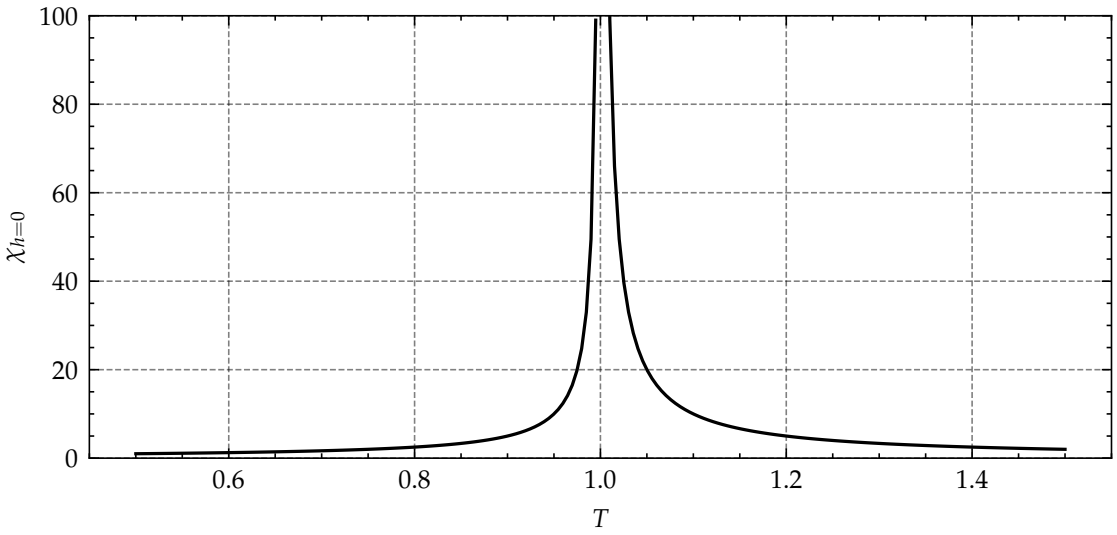

Figure 2.3: Divergence of mean-field susceptibility for $h = 0$ and $T_C = 1$.

Now we can conclude that no matter which way we approach T_C, the susceptibility diverges as

$$\chi \sim |T_C - T|^{-\gamma} \tag{2.25}$$

where $\gamma = 1$ – which is another critical exponent. Now we will use the fact that the free energy is given by

$$\mathcal{F} = -k_B T \ln \mathcal{Z}. \tag{2.26}$$

Combining this with our expression of the mean-field partition function, from Equation (2.12) we get

$$\mathcal{F}_{\mathrm{MF}} = -k_B T \left[-\frac{\beta N q J m^2}{2} + N \ln (2) + N \ln \cosh \beta h_{\mathrm{eff}} \right]. \tag{2.27}$$

If we Taylor expand the last term, neglecting higher powers of h we obtain

$$\mathcal{F}_{\mathrm{MF}} = N k_B T_C \left[-\frac{T}{T_C} \ln (2) + \frac{T - T_C}{T} \frac{m^2}{2} + \left(\frac{T_C}{T} \right)^3 \frac{m^4}{12} - \frac{1}{k_B T} mh + ... \right]. \tag{2.28}$$

This we may generalize to the following form

$$\mathcal{F}_{\mathrm{MF}} = \mathcal{F}_0 + a(T - T_C)m^2 + bm^4 - cmh, \tag{2.29}$$

where a, b and c are constant with respect to the order parameter. Let us now turn our attention to the heat capacity. For $h = 0$, Equation (2.29) has a minimum at $m = 0$ for $T > T_C$ and minima at $m = \pm\sqrt{\frac{-a(T-T_C)}{2b}}$ for $T < T_C$. Consequently, the equilibrium free energy in the two cases becomes

$$\mathcal{F}^*_{\mathrm{MF}} = \begin{cases} \mathcal{F}_0 & T > T_C \\ \mathcal{F}_0 - \frac{a^2(T-T_C)^2}{4b} & T < T_C. \end{cases} \tag{2.30}$$

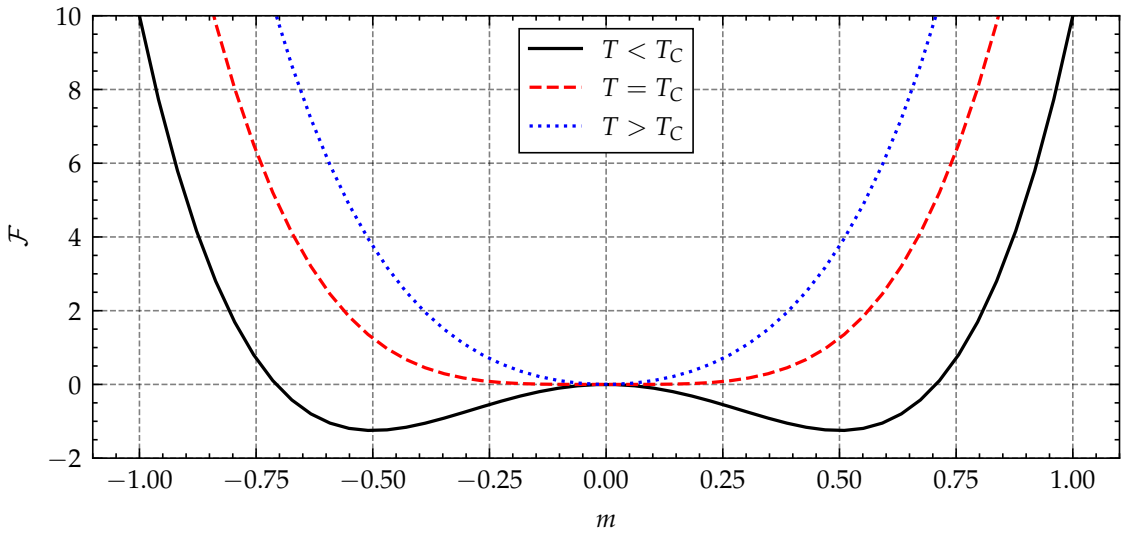

Figure 2.4: Plot of the mean-field free energy as a function of m. Below the critical temperature the free energy has two distinct minima, corresponding to the two possible phases of magnetization. Above the critical temperature the only minima is at $m = 0$, i.e, total disorder. At $T = T_C$, the minimum is also at $m = 0$, but the approach towards the minimum is less steep.

Defining the heat capacity as

$$C = -T\frac{\partial^2 \mathcal{F}}{\partial T^2}, \tag{2.31}$$

we get

$$C = \begin{cases} -T\frac{\partial^2 \mathcal{F}_0}{\partial T^2} & T > T_C \\ -T\frac{\partial^2 \mathcal{F}_0}{\partial T^2} + T\frac{a^2}{2b} & T < T_C \end{cases}. \tag{2.32}$$

Here we see that the heat capacity does not diverge as T approaches T_C, however it does have a discontinuity. Even though the heat capacity does not scale with a power law, we may formally define a critical exponent for the heat capacity as

$$C \sim \lim_{T \to T_C} |T - T_C|^{-\alpha} \implies \alpha = -\frac{\ln(C)}{\ln(|T - T_C|)} = 0. \tag{2.33}$$

In Table 2.1 all critical exponents obtained in this section, as well as the critical temperature, are compared to those of Onsager's exact 2D solution. Apparent is that the mean-field solution fails to accurately determine the value of the critical exponents as well as the location of the phase transition. Nevertheless, mean-field theory does qualitatively capture the essential characteristics of a phase transition – and thus serves as a valuable first stepping stone in the effort to understand critical phenomena.

Table 2.1: Mean-field critical exponents and mean-field critical temperature compared to the Onsager solution of the 2D Ising model.

	α	β	γ	T_C
Mean-field theory	0	1/2	1	Jq/k_B
Onsager's 2D solution ($q = 4$) [19]	0	1/8	7/4	$2J/(k_B \ln(1+\sqrt{2}))$

2.1.3 Limitations of Mean-field Theory

The mean-field Ising model provides a description of phase transitions that is, for the most part, qualitatively correct. In fact, as the dimensionality increases, the mean-field approximation also becomes increasingly more accurate. Moreover, at the *upper critical dimension* the approximation becomes exact. For the Ising model, it is fairly straight-forward to use the *Ginzburg Criterion* to show that the upper critical dimension is $d_{uc} = 4$. Conversely, there also exists a *lower critical dimension*. Below this dimension no phase transition occurs. For the Ising model the lower critical dimension is $d_{lc} = 2$. Consequently, mean-field theory – which predicts a phase transition in low dimensions – fails qualitatively below this point.

So far, we have only discussed thermodynamic quantities derived from the free energy. This, however, does not capture the full picture of a phase transition, as many important physical quantities are related to the correlation of the order parameter rather than its average value alone. As such, we must go beyond the mean-field description.

2.1.4 Beyond Mean-field Theory

Having discussed the limitations of mean-field theory, it is natural to ask: *Can we extend mean-field theory to describe phase transitions in dimensions below $d = 4$?* The most obvious way to improve upon mean-field theory is to modify the free energy, see Equation (2.29), to include terms that account for spatial variations and correlations between spins – effects that were previously neglected in the mean-field approximation. To this end, let us redefine our order parameter as

$$m \equiv \frac{1}{L^d} \int d^d x \, \phi(x), \tag{2.34}$$

where $\phi(x)$ is a continuous field representing the local order parameter density. Later, we will establish a formal connection between this field-theoretic description and the discrete spin lattice of the Ising model. For now, however, we treat $\phi(x)$ as a coarse-grained, continuous approximation that captures the spatial variation of the system. Now we can define a free energy as

$$\mathcal{F} = \int d^d x \, a(T - T_C)\phi(x)^2 + b\phi(x)^4 - c\phi(x)h + d\left(\nabla\phi(x)\right)^2, \tag{2.35}$$

where the term proportional to $(\nabla\phi(x))^2$ captures the spatial variation of the field. But why $(\nabla\phi(x))^2$ and not just $\nabla\phi(x)$? We will now see that the answer lies in symmetry. In the absence of an external field, the free energy must be invariant under $m \to -m$. In the case of the ferromagnet, this is easy to convince oneself of: Equation (2.16) admits one negative and one positive solution, and for spontaneous magnetization one spin direction should not be preferred over the other. When we derived the free energy from mean-field theory, we did not explicitly enforce any symmetries, beyond the construction of the Hamiltonian. However, an alternative approach is to assume only that the free energy is invariant under inversion of the order parameter and to expand it in even powers of the order parameter. This approach – known as *Landau theory* – remarkably reproduces the same form of the free energy as the mean-field Ising model:

$$\mathcal{F}(T) = a(T)m^2 + b(T)m^4 + ..., \tag{2.36}$$

without relying on any microscopic details of the system, suggesting a duality between the Ising model and any other system that is invariant under inversion of the order parameter. At first, this may sound unintuitive, but soon we will see how this notion fits into a greater framework of thought. For now, however, we will focus on understanding the implications of the generalized free energy introduced above, see Equation (2.35), commonly referred to as a ϕ^4- or a *Landau-Ginzburg-Wilson* free energy functional. To this end, we will generalize the external field to having a spatial dependence $h \to h(x)$. Moreover, we will find the equilibrium field configuration by setting the functional derivative of the free energy to zero

$$\begin{aligned}
0 = \delta\mathcal{F} &= \int dx^d \left[\frac{\partial f}{\partial\phi}\delta\phi + \frac{\partial f}{\partial(\nabla\phi)}\delta(\nabla\phi)\right] \\
&= \int dx^d \left[\frac{\partial f}{\partial\phi}\delta\phi - \nabla\cdot\left(\frac{\partial f}{\partial(\nabla\psi)}\right)\delta\phi + \cancel{\nabla\cdot\left(\frac{\partial f}{\partial(\nabla\phi)}\delta\phi\right)}\right] \quad \text{Vanishing surface term} \\
&= \int dx^d \left[\frac{\partial f}{\partial\phi}\delta\phi - \nabla\cdot\left(\frac{\partial f}{\partial(\nabla\phi)}\right)\delta\phi\right] \\
&\implies \left[2a(T-T_C)\phi(x) + 4b\phi(x)^3 - ch(x) - 2d\nabla^2\phi(x)\right] = 0.
\end{aligned} \tag{2.37}$$

In the vicinity of $T = T_C$ the $\phi(x)^3$ can be assumed to be small and can be neglected, as such we can express the following linearized equation

$$\left[a(T-T_C) - d\nabla^2\right]\phi(x) = \frac{c}{2}h(x). \tag{2.38}$$

If we now restrict ourselves to the case when the external field is an impulse at the origin, we can set $\frac{c}{2}h(x) \equiv h_0\delta^{(d)}(x)$ and Equation (2.38) may now readily interpreted as a linear operator acting on a Green's function. To further emphasize this connection, we will by $C(x)$ denote the field configuration/correlation function that solves Equation (2.38)

$$\left[a(T-T_C) - d\nabla^2\right]C(x) = h_0\delta^{(d)}(x), \tag{2.39}$$

and by using the Fourier transform we can easily find the solution to Equation (2.39)

$$C(x) = \int \frac{dk^d}{(2\pi)^d} \frac{h_0 e^{ikx}}{k^2 d + a(T - T_C)}, \tag{2.40}$$

which for $d = 3$ simply becomes

$$C(x) = \frac{h_0/d}{4\pi} \frac{1}{r} e^{-r/\xi}, \; \xi = \left(\frac{a}{d}(T - T_C)\right)^{-\nu}, \tag{2.41}$$

where $\nu = \frac{1}{2}$. Thus we have found yet another critical exponent – this one describes the divergence of the spin-spin correlation length, ξ, as $T \to T_C$.

2.1.5 Critical Exponent Identities

Starting from the mean-field Ising model, and investigating its thermodynamic quantities as $T \to T_C$, we discovered three different critical exponents: α, β and γ. α and γ characterize the divergence of the heat capacity and the susceptibility as the temperature approaches the critical temperature – while β quantifies the decay of the order parameter as the critical temperature is approached from below. These exponents, we found, are valid for all systems that are symmetric under the inversion of the order parameter, not just the Ising model.

By coarse graining, i.e. defining the global order parameter as the integral over a local order parameter density field, and including a term capturing spatial variation in the Landau free energy, we could derive a final critical exponent ν, which characterizes the divergence of the correlation length at criticality.

This list of critical exponents is not exhaustive, in theory any number of critical exponents could be conceived of by considering high order derivatives of thermodynamic quantities – however two of the most common equilibrium critical exponents yet to be mentioned are δ and η. δ relates the order parameter to the external field at criticality

$$m \sim |h|^{1/\delta}, \tag{2.42}$$

and η governs the decay of the correlation function at criticality

$$C(r) \sim r^{-d+2-\eta}. \tag{2.43}$$

Since the different thermodynamic quantities (except for the correlation length) all ultimately are derived by differentiating the free energy with respect to T or h, it is not unfounded to suspect that the exponents should be related to each other somehow. We will expand upon this notion by generalizing some of the results above. Let us first revisit Landau's expansion in m

$$f_{\mathrm{MF}} = a\tau m^2 + bm^4 - cmh, \tag{2.44}$$

where $\tau \equiv \frac{T - T_C}{T_C}$ (and a factor T_C has been absorbed into a). Here we use the notation f_{MF} to emphasize that we are working with the *free energy density*, an

intensive quantity. For $\partial_m f = 0$ the free energy density has minima, solving for the limits $\tau \to 0$ and $h \to 0$ gives us

$$f^{\min}_{\mathrm{MF},h\to 0} \sim -\tau^2 \tag{2.45}$$

and

$$f^{\min}_{\mathrm{MF},\tau\to 0} \sim -h^{4/3}. \tag{2.46}$$

Knowing this, we can construct a homogenous function[1] that captures the behavior of the free energy density

$$f_{\mathrm{MF}}(\tau, h) = |\tau|^2 g_f\left(\frac{h}{|\tau|^\Delta}\right), \tag{2.47}$$

where $\Delta = 3/2$, $\lim_{x\to 0} g_f(x) = \text{const.}$ and $\lim_{x\to\infty} g_f(x) \sim x^{4/3}$ to recover the limits of the control parameters above. We may now generalize this expression beyond the mean-field approximation, for systems where α does not necessarily have to equal 0 (and Δ need not be $\frac{3}{2}$),

$$f(\tau, h) = |\tau|^{2-\alpha} g_f\left(\frac{h}{|\tau|^\Delta}\right). \tag{2.48}$$

The notion that the free energy, in general, may be expressed by a homogeneous function is sometimes called the *homogeniety assumption*. This assumption was first introduced by Widom in 1965, then in the context of van der Waals fluids [20]. From Equation (2.48) it is straightforward to calculate relevant thermodynamic quantities. For instance, the order parameter may be defined as the derivative of the free energy density with respect to the external field

$$m \equiv \frac{\partial f}{\partial h} \sim |\tau|^{2-\alpha-\Delta} g_m\left(\frac{h}{|\tau|^\Delta}\right), \tag{2.49}$$

where $g_m \equiv \partial_h g_f$ is a new homogeneous function. Consequently, we get

$$m(\tau, h = 0) \sim |\tau|^{2-\alpha-\Delta} \implies \beta = 2 - \alpha - \Delta, \tag{2.50}$$

but also

$$m(\tau \to 0, h) = |\tau|^{2-\alpha-\Delta}\left(\frac{h}{|\tau^\Delta|}\right)^p. \tag{2.51}$$

where $p\Delta = 2 - \alpha - \Delta$ since the τ-dependence should vanish. As such we get

$$m(\tau \to 0, h) \sim h^{(2-\alpha-\Delta)/\Delta} \implies \delta = \Delta/(2 - \alpha - \Delta). \tag{2.52}$$

Similarly, the susceptibility can be expressed as

$$\chi = \frac{\partial m}{\partial h} \sim |\tau|^{2-\alpha-2\Delta} g_\chi\left(\frac{h}{|\tau|^\Delta}\right) \tag{2.53}$$

[1] A homogenous function f of order k, is one that satisfies $f(sx) = s^k f(x)$.

where $g_\chi \equiv \partial_h g_m$, and we get the following relation

$$\chi(\tau, h=0) \sim |\tau|^{2-\alpha-2\Delta} \implies \gamma = 2-\alpha-2\Delta. \tag{2.54}$$

Remarkably we see that β, δ and γ all can be expressed by the two independent exponents α and Δ. Moreover, combining the expressions for the critical exponents in Equations (2.50), Equation (2.52) and Equation (2.53) gives us the following identities

$$\alpha + 2\beta + \gamma = 2 \tag{2.55}$$

and

$$\delta = 1 + \frac{\gamma}{\beta} \tag{2.56}$$

which are known as *Rushbrooke's Identity* [21] and *Widom 's Identity* [22], named after the scientists that first proposed them. To derive the remaining two critical exponents, ν and η, which are not directly related to the free energy density, we may pose a similar ansatz for the correlation length:

$$\xi \sim |\tau|^{-\nu} g_\xi \left(\frac{h}{|\tau|^\Delta} \right). \tag{2.57}$$

In addition, we demand that:

> At criticality – the correlation length should be the only length scale that contributes to thermodynamic singularities.

The second condition implies that the logarithm of the partition function, which importantly is both *extensive and dimensionless*, has to be of the following form

$$\ln \mathcal{Z} = \left(\frac{L}{\xi} \right)^d g_x + \left(\frac{L}{a} \right)^d g_a + ..., \tag{2.58}$$

where $g_{...}$ are dimensionless functions that do not give rise to singularities, and a is some microscopic length scale of the system. As such, the first term must capture the singular behavior, while the remaining terms encode only subleading, non-singular corrections. Consequently, we can relate the free energy density to the correlation length

$$f \sim \frac{\ln \mathcal{Z}}{L^d} \sim \frac{1}{L^d} \left(\frac{L}{\xi} \right)^d \sim |\tau|^{d\nu} g_\xi \left(\frac{h}{|\tau|^\Delta} \right) \tag{2.59}$$

and obtain a new exponent identity

$$2 - \alpha = \nu d, \tag{2.60}$$

which is known as *Josephson's Identity* [23]. Lastly, we can extract one final exponent identity by expressing the susceptibility as the spatial integral over the

correlation function. For $r \gg \xi$ the correlation function vanishes exponentially, and as such, we can set the upper integration bound to ξ to study the power-law behavior of the correlation function. Consequently, we find

$$\chi \sim \int_0^{\xi} d^d r \, r^{-d+2-\eta} \sim \xi^{2-\eta} \sim |\tau|^{-\nu(2-\eta)} \tag{2.61}$$

and we retrieve

$$\gamma = \nu(2-\eta), \tag{2.62}$$

which is known as *Fisher's Identity* [24].

2.1.6 Universality Classes

In the previous section we saw that the critical exponents were interrelated through exponent identities (also known as *scaling laws*). This is a convenient result – the exponents represent measurable quantities and as such an experimentalist would only need to extract two exponents to fully characterize the critical behaviour of a system. Since a vast number of different physical systems undergo phase transitions – a naive assumption would be that there exists equally many sets of critical exponents. This however is not the case – there are actually only around $\mathcal{O}(10^1)$ distinct, physically realizable universality classes [25]. This should come as no surprise. In previous sections we argued that all systems which were invariant under order parameter inversion should exhibit a free energy of the same form. Moreover, we know that some of the exponent identities have an explicit dependence on dimensionality. As such we may conjecture that there exist far fewer sets of critical exponents than the number of phase transitions – and that the values of the exponents are solely dependent on the symmetries and dimensionality of the phase transition. More concisely, the *Universality Hypothesis* states:

> All phase transitions, characterized by their sets of critical exponents, fall into a finite number of classes, uniquely determined by the dimensionality of the system d and the dimensionality of the order parameter n [26].

These classes, commonly referred to as *Universality Classes* contain many curious connections. For instance, the Ising model is in the same universality class as the liquid-vapor transition, two systems that share no microscopic similarities [27]. Likewise, the 3D XY model, originally a model for planar magnets, shares universality class with the superfluid transition of Helium-4 [28].

2.2 Finite-size Scaling Theory

To numerically compute critical exponents is generally not as easy as it may seem at first. The fundamental issue that arises is that we should only expect thermodynamic properties to adhere to critical scaling in the thermodynamic limit, i.e.

when $L^d = V \to \infty$. For numerical studies, the size of the lattice is finite. Naturally, with abundant computational resources, we may simulate sufficiently large lattices and get acceptable estimates of the critical exponents anyhow; however, we will see that there exists a far more computationally tractable approach that actually leverages the limitations that finite-size systems incur.

2.2.1 The Finite-size Scaling Hypothesis

At the thermodynamic limit we expect critical fluctuations of the system to be correlated over a length scale given by ξ. Let us now suppose that some dimension of the system is finite with a length given by L. When the finite dimension is significantly smaller than the correlation length, $L \ll \xi$, the correlation length is effectively saturated to L. Consequently long range correlations are absent and fluctuations are suppressed. Moreover, we don't expect a proper phase transition in this regime. In the case that $L \gg \xi$, we don't expect to see any finite size effects and the thermodynamic properties of the systems are unaffected by the finite dimension. However, at the critical point, where we observe the critical scaling, the correlation length ξ diverges ($\xi \to \infty$). Thus we can never pick a finite lattice size that is sufficiently large to capture the true critical scaling of the system at the critical point. As such, we should only expect to see meaningful finite size effects when the correlation length is on the same order as the system size, $\xi \approx L$. Let us revisit Equation (2.59), where the free energy density was related to the homogenous scaling function of the correlation length and the reduced temperature

$$f \sim |\tau|^{d\nu} g_\xi \left(\frac{h}{|\tau|^\Delta} \right). \tag{2.63}$$

Since near criticality

$$|\tau|^{-\nu} \sim \xi \sim L \tag{2.64}$$

and we can express the free energy density as

$$f \sim L^{-(2-\alpha)/\nu} g_f \left(L^{1/\nu}|\tau|,\, L^{\Delta/\nu} h \right), \tag{2.65}$$

where we made use of Josephson's Identity. Moreover, we have made explicit the dependence on a dimensionless factor $L^{1/\nu}|\tau|$ that quantifies the distance from the critical point. Comparing Equation (2.65) with Equation (2.48), any thermodynamic quantity ζ (with a critical exponent θ) derived from the free energy density will have the following form

$$\zeta = L^{-\theta/\nu} g_\zeta \left(L^{1/\nu}|\tau|,\, L^{\Delta/\nu} h \right). \tag{2.66}$$

This is an ansatz which we may call the *finite-size scaling hypothesis*, even though it follows directly from the homogeneity assumption of the correlation length. The implications of this new expression are however profound. Instead of calculating the critical exponent explicitly, i.e. by fitting a power law to ζ at criticality, we may now simulate the system for different values of L and observe how the value of ζ scales with L at criticality. Moreover, we also expect the location of

the critical point to shift with system size. Consequently, the term *pseudocritical point* is often used to denote the point where finite-size systems undergo a phase transition, and the true critical point is only approached in the thermodynamic limit. This is a result of the fact that the crossover point where the correlation length is comparable to system size is itself subject to finite-size effects

$$\tau \sim L^{-1/\nu} \implies T \sim T_C + cL^{-1/\nu}. \tag{2.67}$$

As such, by fitting a power law to the location of the pseudocritical point for different system sizes, we may extract the location of the true critical point and an independent estimate of the exponent ν. In practice, the estimation of pseudocritical points can be hard since phase transitions by nature are less pronounced in finite-size systems.

2.2.2 Estimating the Critical Point

An alternative approach to estimating ν and τ_c is to calculate the Binder cumulant. Introduced by Kurt Binder in 1981 [29], the Binder cumulant is given by

$$U = 1 - \frac{\langle M^4 \rangle}{3\langle M^2 \rangle^2}, \tag{2.68}$$

i.e. the excess kurtosis of M, divided by -3. The physical interpretation of this expression is of secondary nature to its usefulness in determining the point of phase transition. The Binder cumulant scales weakly with system size at the critical point, and thus in the context of a finite size scaling analysis, the critical point is often taken to be the point of intersection between the cumulants corresponding to the largest and second largest systems simulated.

2.3 Microscopic Derivation of Landau-Ginzburg-Wilson Free Energy

In previous sections we have discussed the connection between the Ising model and the ϕ^4-model through the mean-field approximation followed by a coarse-graining step. To further emphasize this connection we will now see that the ϕ^4/Landau-Ginzburg-Wilson free energy can be directly derived from a general Ising Hamiltonian,

$$H_{\text{Ising}} = -\sum_{ij} J_{ij} s_i s_j, \tag{2.69}$$

where J_{ij} is a translationally invariant correlation matrix that describes the interaction of the spins. An alternative approach to the mean-field approximation is to perform a so-called Hubbard-Stratonovich transformation, which resolves the interaction of the spins at the cost of introducing an auxiliary scalar order parameter field, ϕ. For tractability, we have omitted external magnetic fields, but the derivations below can easily be generalized to also admit a non-zero external

field. Let us motivate this transformation by first revisiting the solution of a 1D Gaussian integral, where $a > 0$:

$$\sqrt{\frac{\pi}{a}} = \int_{-\infty}^{\infty} dx\, e^{-a\left(x-\frac{b}{a}\right)^2} = \int_{-\infty}^{\infty} dx\, e^{-ax^2+2bx-\frac{b^2}{a}}. \tag{2.70}$$

Rearranging the terms we may express

$$e^{\frac{b^2}{a}} = \sqrt{\frac{a}{\pi}} \int_{-\infty}^{\infty} dx\, e^{-ax^2+2bx}. \tag{2.71}$$

Let us further generalize this expression by letting b and x be vectors s and ψ, $b \to s_i$, $x \to \psi_i$ and $1/a$ be a matrix J, $\frac{1}{a} \to \beta J_{ij}$, with inverse $(\beta J_{ij})^{-1}$. Consequently Equation (2.71) may now be written as

$$e^{\beta \sum_{ij} J_{ij} s_i s_j} = \frac{1}{\sqrt{\det(4\pi\beta J)}} \int_{-\infty}^{\infty} D\psi\, e^{-\sum_{ij} \psi_i (\beta J_{ij})^{-1} \psi_j + 2\sum_i s_i \psi_i}. \tag{2.72}$$

Letting $\mathcal{N} \equiv \frac{1}{\sqrt{\det(4\pi\beta J)}}$, the partition function takes the following form

$$\mathcal{Z} = \mathcal{N} \int_{-\infty}^{\infty} D\psi \sum_{\{s_i\}} e^{-\sum_{ij} \psi_i (\beta J_{ij})^{-1} \psi_j + 2\sum_i s_i \psi_i} \tag{2.73}$$

where we no longer have a spin-spin interaction term! Thus we can easily perform the summation over spins

$$\mathcal{Z} = \mathcal{N} \int_{-\infty}^{\infty} D\psi\, e^{-\sum_{ij} \psi_i (\beta J_{ij})^{-1} \psi_j} \prod_i 2\cosh 2\psi_i, \tag{2.74}$$

where we will absorb a factor $\prod_i 2$ into $\mathcal{N}$. If we change the variable of integration to $\phi_i = \sum_j (\beta J_{ij})^{-1} \psi_j$, rearrange and absorb any factors related to the change of variables into $\mathcal{N}$, we end up with

$$\mathcal{Z} = \mathcal{N} \int_{-\infty}^{\infty} D\phi\, e^{-\sum_{ij} \phi_i (\beta J_{ij}) \phi_j + \sum_i \ln(\cosh(\sum_j 2\beta J_{ij} \phi_j))}. \tag{2.75}$$

From here on we will focus on the action, i.e. (minus) the argument of the exponential, and also make the assumption that we are working at low temperatures. Consequently, $\beta = \frac{1}{k_B T}$ will have a high value and suppress fluctuations of ϕ, thus we may perform a Fourier expansion of the field and the correlation matrix. By then Taylor expanding $\ln(\cosh(...))$, transforming back to position-space and taking the continuum limit we get

$$S[\phi] = \int d^d x\, c_1 (\nabla\phi)^2 + c_2 \phi^2 + c_3 \phi^4 \tag{2.76}$$

where $c_1 = \frac{\beta}{2} J''(0)\,(1 - 4\beta J(0))$, $c_2 = \beta J(0)\,(1 - 2\beta J(0))$ and $c_3 = \frac{4\beta^4}{3} J(0)^4$ [2]. Although somewhat more obtuse at first, we see that the form of the quadratic

[2] See Appendix A for full derivation.

coefficient in the free energy implies a phase transition, just like in the mean-field case. Since $J(0)$ has to be positive, c_2 will switch sign at $T = 2J(0)/k_B$. To conclude, from this derivation we have shown the direct connection between the Ising model and ϕ^4-theories. In Figure 2.5, a roadmap of the different methods used in this thesis to derive the ϕ^4-model is illustrated.

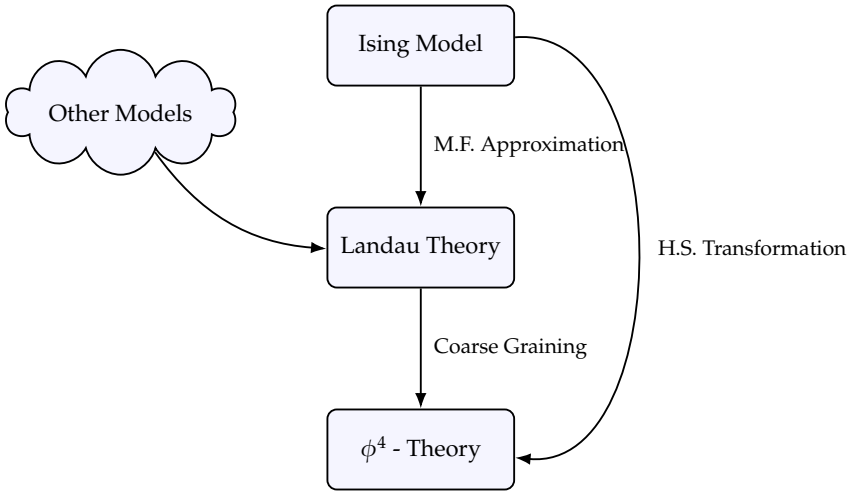

Figure 2.5: Sketch illustrating the connection between the Ising model, Landau theory and ϕ^4-theory.

2.4 Time-dependent Ginzburg-Landau Theory

As of yet we have only considered the static behavior of the ϕ^4-model. A natural next step would be to extend the model to also encompass time-dependent fluctuations near equilibrium. A reasonable (and phenomenological) assumption would be that the relaxation rate of ϕ is proportional to the deviation from equilibrium of the free energy, $\frac{\delta \mathcal{F}}{\delta \phi}$. This description is not quite correct. The free energy function need not necessarily be convex, and thus the order parameter may evolve to a *local* minimum, however, the equilibrium state should always correspond to the *global* minimum. To remedy this we will, in analogy to stochastic optimization, introduce some noise η. Consequently, the *time dependent Ginzburg-Landau* (TDGL) equation becomes

$$\partial_t \phi(x,t) = -\gamma \frac{\delta \mathcal{F}[\phi]}{\delta \phi(x,t)} + \eta(x,t), \tag{2.77}$$

where γ is some phenomenological relaxation constant. The physical interpretation of η is that the term represents the thermal fluctuations inherent to the system due to its microscopic degrees of freedom [30]. Moreover, the noise is assumed to be Gaussian

$$P_\eta \sim \exp\left[-\frac{1}{q}\int dt\, dx^d\, \eta(x,t)^2\right], \tag{2.78}$$

with $\langle \eta(x,t) \rangle = 0$ and $\langle \eta(x,t)\eta(x',t') \rangle = q\delta(x-x')\delta(t-t')$, i.e. uncorrelated in time and space. Here the angle brackets denote ensemble averages.

Since we used very general assumptions to motivate Equation (2.77), it should come as no surprise that many expressions of similar or functionally equivalent form are known in physics. These are most often referred to as overdamped Langevin dynamics, but in the context of superfluids, a closely related equation is known as the (stochastic) Gross-Pitaevskii equation [31], and in critical dynamics it is commonly known as *model A* [32]. Lastly, we note that the probability distribution of the TDGL dynamics obeys the Fokker-Planck equation

$$\partial_t P = \gamma \int dx^d \left[\frac{\delta P}{\delta \phi(x,t)} + P \frac{\delta \mathcal{F}[\phi]}{\delta \phi(x,t)} \right], \tag{2.79}$$

and as such the equilibrium distribution of the TDGL dynamics will be the Boltzmann distribution associated with the ϕ^4-free energy functional [32]

$$P_{\text{eq}} \propto e^{-\beta \mathcal{F}[\phi]}. \tag{2.80}$$

Consequently, the TDGL dynamics is not only useful for probing the behaviour of the field out of equilibrium – if we let the field evolve according to the TDGL equation for sufficiently long times we should in theory recover the static equilibrium behaviour associated with the ϕ^4-model. As such, TDGL simulations can serve as an alternative to both static and kinetic Monte Carlo schemes.

One important distinction to be made is that upon the inclusion of noise, the phase transition will no longer occur at $\tau = 0$ [33]. In practice, the coefficient of the quadratic term in the free energy will be shifted

$$... + \alpha\tau\phi^2 + ... \rightarrow ... + \alpha(\tau - \tau_C)\phi^2 + ... \tag{2.81}$$

so that the phase transition now occurs at an effective critical point $\tau = \tau_C$.

2.4.1 Fluctuation-dissipation Theorem

If we want to use the TDGL equation to probe the critical behaviour of thermodynamic quantities, it is essential that we make clear the temperature dependence of the noise-noise correlator q. For a Ginzburg-Landau-Wilson free energy functional with zero external field

$$\mathcal{F}[\phi] = \int dx^d \left[\tau\alpha\phi(x,t)^2 + \beta\phi(x,t)^4 + (\xi_0 \nabla \phi(x,t))^2 \right], \tag{2.82}$$

the corresponding TDGL equation is

$$\partial_t \phi(x,t) = -\gamma \left[2\alpha\tau\phi(x,t) + 4\beta\phi(x,t)^3 - 2\xi_0^2 \nabla^2 \phi(x,t) \right] + \eta(x,t), \tag{2.83}$$

where $\langle \eta(x,t) \rangle = 0$ and $\langle \eta(x,t)\eta(x',t') \rangle = q\delta(x-x')\delta(t-t')$. For the sake of simplicity, we will now restrict the free energy functional to only the ϕ^2-term.

Near criticality, this approximation is valid since in that regime, we expect the order parameter to be small and, as such, the term linear in ϕ will be leading. Equation (2.83) now becomes

$$\partial_t \phi(x,t) = -2\gamma\alpha\tau\phi(x,t) + \eta(x,t). \tag{2.84}$$

This enables us to derive an analytical expression for q. In the long time limit the ensemble average may be approximated with a time average

$$\langle A(x,t)\rangle \approx \frac{1}{\mathcal{T}_0}\int_{t-\frac{\mathcal{T}_0}{2}}^{t+\frac{\mathcal{T}_0}{2}} A(x,s)\,ds, \tag{2.85}$$

where $\mathcal{T}_0$ is a time much longer than the characteristic time scale of the system but also $\mathcal{T}_0 << \mathcal{T} = \frac{1}{\gamma}$. Solving equation (2.84) gives us

$$\phi(x,t) = \phi_0(x)e^{-2\gamma\alpha\tau t} + \int_0^t ds\, e^{-2\gamma\alpha\tau(t-s)}\eta(x,s), \tag{2.86}$$

which we may plug into Equation (2.85) and thus obtain

$$\langle\phi(x,t)\rangle = \phi_0(x)e^{-2\gamma\alpha\tau t}. \tag{2.87}$$

In a similar fashion, we may obtain the mean square fluctuations

$$\begin{aligned}\phi(x,t)^2 = \phi_0(x)^2 e^{-4\gamma\alpha\tau t} + 2\phi_0(x)e^{-2\gamma\alpha\tau t}\int_0^t ds\, e^{-2\gamma\alpha\tau(t-s)}\eta(x,s) \\ + \int_0^t ds\int_0^t ds'\, e^{-2\gamma\alpha\tau(2t-s-s')}\eta(x,s)\eta(x,s')\end{aligned} \tag{2.88}$$

and the average squared velocity

$$\langle\phi(x,t)^2\rangle = \phi_0(x)^2 e^{-4\gamma\alpha\tau t} + \frac{q}{4\gamma\alpha\tau}\left[1 - e^{-2\gamma\alpha\tau t}\right]. \tag{2.89}$$

For long time scales, i.e. $t \to \infty$, the mean squared fluctuations go to $\langle\phi^2\rangle \to \frac{q}{4\gamma\alpha\tau}$. By means of the equipartition theorem we may express the average energy of the field at every point as

$$\left\langle \alpha\tau\phi(x,t)^2 \right\rangle = \frac{k_B T}{2}. \tag{2.90}$$

Consequently, we obtain the following equality

$$q = 2\gamma k_B T. \tag{2.91}$$

This result is known as the fluctuation-dissipation theorem. In its most general form, the theorem relates the impedance in a linear dissipative system to the fluctuations of the associated forces [34]. In Equation (2.91) we see that the existence of dissipative forces proportional to γ, i.e. $(\frac{\delta\mathcal{F}}{\delta\phi})$, implies the existence of fluctuations q, and vice versa.

2.5 Stochastic Thermodynamics

The field of thermodynamics traces its origin to the mid 19th century. At the time, the industrial revolution was nearing its apex, and the rapid industrialization of the western world had suddenly facilitated a host of urgent and practical questions that engineers and physicists sought to answer. Specifically – the steam engine was of great interest. Originally the catalyst of the industrial revolution itself – the theoretical study of steam engine efficiency came to be the start of the field of thermodynamics [35]. In this effort, one of the most important quantities in the field of thermodynamics was introduced, namely *entropy*.

First coined by Clausius in 1865 [36], entropy is a measure of the energy that cannot be converted into work in a closed system – an idea closely linked to the finite efficiency and dissipation of heat in steam engines [37]. Clausius defined the change in entropy ΔS, as being greater than or equal to the quotient between the heat exchange ΔQ, and the absolute temperature T

$$\Delta S \geq \frac{\Delta Q}{T}, \tag{2.92}$$

where the equality holds only for reversible processes. Later, Ludwig Boltzmann came to give entropy its statistical interpretation as being proportional to the logarithm of the number of possible configurations of a system Ω – also known as microstates

$$S \equiv k_B \ln \Omega. \tag{2.93}$$

The field of *stochastic thermodynamics* is an extension of the traditional thermodynamics discussed above. Being a relatively young field, it was first introduced in the 1990s in the study of systems such as colloidal particles, molecular motors and biopolymers [38]. The main difference between traditional thermodynamics and stochastic thermodynamics is that observables in traditional thermodynamics are macroscopic, and fluctuations will be on the order of $\mathcal{O}(V)$, V being the volume of the system. Consequently, two states that differ from each other by less than $\mathcal{O}(V)$ are considered thermodynamically equivalent. Stochastic thermodynamics, on the other hand, admits microscopic observables at arbitrarily high resolution. Moreover, in stochastic thermodynamics, the macroscopic state is replaced by a probability distribution over microscopic states [39]. In the following subsection, we will introduce one of the central quantities in stochastic thermodynamics: *entropy production*.

2.5.1 Entropy Production

In equilibrium, physical systems exhibit an invariance under time-reversal transformations. More concretely, detailed balance is observed

$$p[\{x\}|x_0]\pi(x_0) = p^\dagger[\{x\}|x_T]\pi(x_T), \tag{2.94}$$

where $p[\{x\}|x_0]$ denotes the path probability of a trajectory $\{x(t)\}_{t=0}^{T}$ conditioned on an initial value x_0, $p^\dagger[\{x\}|x_T]$ denotes its time-reversed counterpart

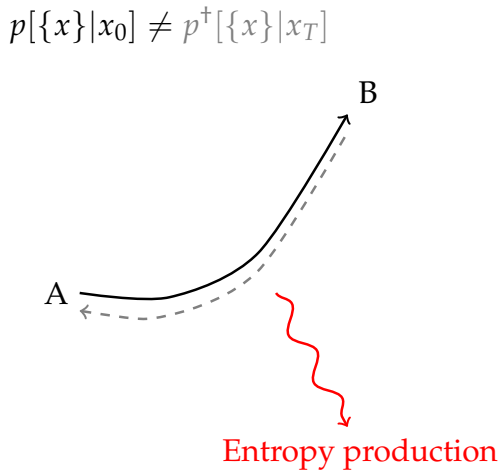

Figure 2.6: Sketch illustrating the entropy production of an irreversible trajectory. When the path probability of the forward trajectory differs from that of the time-reversed trajectory, entropy is produced.

conditioned on the final value x_T and $\pi(x)$ is the corresponding stationary distribution. Beyond equilibrium this does, however, not hold. Moreover, the extent to which this equality is broken tells us how irreversible a certain process is and how far the corresponding system is from the equilibrium regime. Along these lines we may define the following quantity

$$\Sigma \equiv k_B \ln \frac{p[\{x\}|x_0]}{p^\dagger[\{x\}|x_T]}, \tag{2.95}$$

which is the *entropy production* of a trajectory [40]. In the case of a scalar field $\phi(x,t)$ propagated by Langevin dynamics, the probability of the field trajectories may not necessarily be directly accessible. As such, it is advantageous to switch to a path integral representation of the dynamics. For the TDGL equation, we may express the noise field as

$$\eta(x,t) = \frac{1}{\sqrt{q}}\left[\partial_t \phi(x,t) + \gamma \frac{\delta \mathcal{F}[\phi]}{\delta \phi(x,t)}\right], \tag{2.96}$$

where we made the magnitude of the noise explicit by including a factor $\sqrt{q}$. Furthermore, since the noise field is Gaussian and uncorrelated in time and space, we may express the probability of a noise trajectory, given an initial noise η_0, as

$$p\left[\{\eta\}|\eta_0\right] \sim e^{-\frac{1}{2}\int dt\, dx\, \eta(x,t)^2}. \tag{2.97}$$

Since the mapping between field and noise $\eta \mapsto \phi$ is purely deterministic, any field trajectory with given initial conditions can be uniquely determined from a realization of the noise. In practice, this means that the probability of the field trajectories is proportional to that of the noise trajectories [8]

$$p\left[\{\phi\}|\phi_0\right] \sim p\left[\{\eta\}|\eta_0\right], \tag{2.98}$$

which enables us to express the associated entropy production as

$$\Sigma[\phi] = k_B \ln \frac{p\left[\{\phi\}|\phi_0\right]}{p^\dagger\left[\{\phi\}|\phi_T\right]} = -\frac{k_B}{2}\int dt\, dx \left[\eta(x,t)^2 - \eta^\dagger(x,t)^2\right]. \tag{2.99}$$

The only terms which will not cancel are the terms that are odd under time reversal. Consequently, we are left with

$$\Sigma\left[\phi\right] = \frac{1}{2T}\int dt\, dx \left\langle -\partial_t\phi(x,t)\frac{\delta\mathcal{F}[\phi]}{\delta\phi(x,t)}\right\rangle, \tag{2.100}$$

where we through $\langle ... \rangle$ have made explicit that the entropy production is obtained by averaging over trajectories. For the case when the field is coupled to an external, time-dependent field $F^{\text{ext}}(t)$ we may decompose the free energy into

$$\mathcal{F}[\phi] = \mathcal{F}^{\text{Eq.}}[\phi] - \phi(x,t)F^{\text{ext}}(t), \tag{2.101}$$

such that the entropy production becomes

$$\Sigma\left[\phi\right] = \frac{1}{2T}\left[\cancel{-\left\langle \Delta\mathcal{F}^{\text{Eq.}}\right\rangle} + \int dt\, dx \left\langle \partial_t\phi(x,t)F^{\text{ext}}(t)\right\rangle\right], \tag{2.102}$$

where the term $\langle \Delta\mathcal{F}^{\text{Eq.}}\rangle \equiv \langle \mathcal{F}^{\text{Eq.}}(t_{\text{Final}}) - \mathcal{F}^{\text{Eq.}}(t_0)\rangle$ is neglected to focus on the direct contribution to the entropy production of the external field. Moreover, this term will for a periodic drive be bounded, and will vanish upon long time averaging [12]. As such, the final expression for the entropy production becomes

$$\Sigma\left[\phi\right] = \frac{1}{2T}\int dt\, dx \left\langle \partial_t\phi(x,t)F^{\text{ext}}(t)\right\rangle. \tag{2.103}$$

In Figure 2.7 the entropy production of a field coupled to an external drive is illustrated.

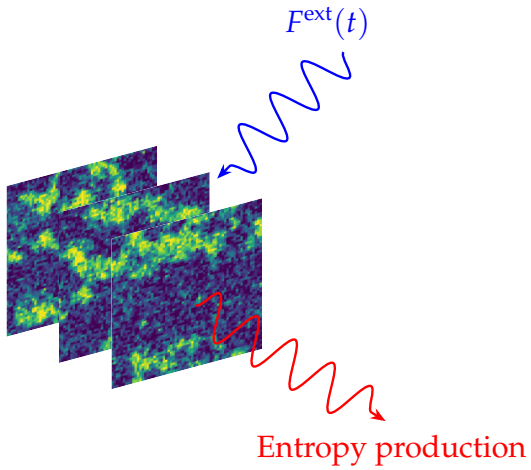

Figure 2.7: Sketch illustrating the entropy production (in red) of a scalar order parameter field coupled to an external field (in blue).

3
Methods

To study the critical nature of entropy production, numerical simulations of the TDGL equation are performed. As a validation of the numerical implementation of the model, equilibrium critical exponents, α, β, γ and ν are extracted and compared to known theoretical values, for a 2D and a 3D lattice.

3.1 Solving the TDGL Equation

To numerically solve the TDGL equation, the python library `py-pde` has been used. `py-pde` employs finite-difference time-domain methods to solve partial differential equations as well as stochastic partial differential equations. For stochastic partial differential equations, the solver uses the explicit Euler-Maruyama method [41]

$$\phi(x, t + \Delta t) = \phi(x, t) - \Delta t \gamma \frac{\delta \mathcal{F}(t)}{\delta \phi(x, t)} + \sqrt{\Delta t} \sqrt{q} \eta(x, t), \tag{3.1}$$

where the timestep has been set to $\Delta t = 0.01$, for all simulations. The initial field configurations are drawn from a uniform distribution $\phi(x, t = 0) \sim \mathcal{U}[-0.5, 0.5]$, and periodic boundary conditions are enforced $\phi(x + L, t) = \phi(x, t)$. Moreover, the parameters of the free energy are set to $\alpha = 2\beta = 2(\xi_0)^2 = \frac{1}{2\gamma}$ such that the dissipative force becomes

$$\gamma \frac{\delta \mathcal{F}(t)}{\delta \phi(x, t)} = \tau \phi(x, t) + \phi(x, t)^3 - \frac{1}{2} \nabla^2 \phi(x, t), \tag{3.2}$$

for equilibrium simulations and

$$\gamma \frac{\delta \mathcal{F}(t)}{\delta \phi(x, t)} = \tau \phi(x, t) + \phi(x, t)^3 - \frac{1}{2} \nabla^2 \phi(x, t) - F^{\text{ext}}(t), \tag{3.3}$$

for non-equilibrium simulations. The magnitude of the noise is related to the control parameter τ by

$$q = 2\gamma k_B T = 2(1 + \tau)\Gamma \tag{3.4}$$

where $\Gamma = 0.861$.

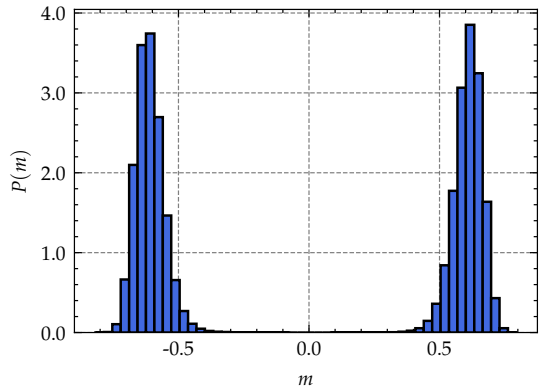

(a) In the ordered phase $P(m)$ is a bimodal distribution.

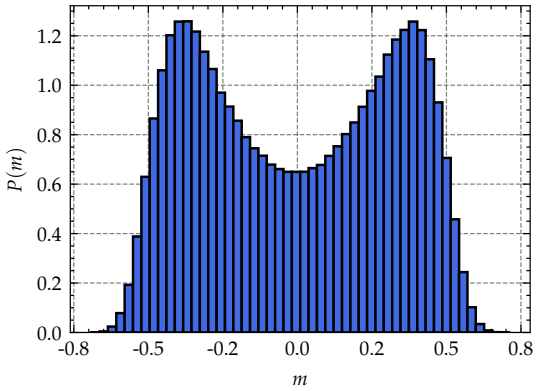

(b) Near criticality $P(m)$ approaches a unimodal distribution centered at $m = 0$.

Figure 3.1: Probability distributions of the instantaneous order parameter, m, in **(a)** the ordered phase and **(b)** near criticality, for a 16x16 lattice.

3.2 Meaningful Observables

For finite-size systems, the instantaneous magnetization

$$m \equiv \frac{1}{L^d} \sum_i \phi_i \tag{3.5}$$

will, during the course of a simulation, occasionally flip between opposite phases $m \to -m$. Thus the time average of the magnetization $M \equiv \langle m \rangle$ will vanish even in the ordered phase, $M = \langle m \rangle = 0$, as illustrated in Figure 3.1. To remedy this we may define $|M| \equiv \langle |m| \rangle$ as our new order parameter, which does not vanish in the ordered phase, $M \neq 0$. Since the magnetic susceptibility is defined as

$$\chi_M = \frac{\partial M}{\partial h}, \tag{3.6}$$

we could apply an external field and calculate the rate of change of M for varying field strengths. An alternative way is to instead calculate

$$\chi_M = \frac{\partial M}{\partial h} = \frac{\partial \langle m \rangle}{\partial h} = \frac{\partial}{\partial h} \left[\frac{\mathrm{Tr}(m e^{-\beta H})}{\mathcal{Z}} \right] = L^d \beta \left[\langle m^2 \rangle - \langle m \rangle^2 \right], \tag{3.7}$$

which is another manifestation of the fluctuation-dissipation theorem. Moreover, this expression is also valid in the absence of an external field. Since we used $|M|$ as the order parameter, we may, for consistency, define the magnetic susceptibility as

$$\chi_{|M|} = L^d \beta \left[\langle m^2 \rangle - \langle |m| \rangle^2 \right], \tag{3.8}$$

which, in a strict sense is not the "true" magnetic susceptibility, χ_M. $\chi_{|M|}$ will, however, in the thermodynamic limit be equivalent to χ_M and will exhibit equivalent finite-size scaling properties. The advantage of calculating $\chi_{|M|}$ instead of

χ_M is that the former will be less "noisy" for finite time simulations. Similarly, we may also use the fluctuation-dissipation theorem to express the heat capacity as

$$C = \frac{L^d \beta}{T} \left[\langle E^2 \rangle - \langle E \rangle^2 \right], \tag{3.9}$$

where $E \equiv \frac{1}{L^d} \sum \mathcal{F}$ is the instantaneous mean of the free energy field. To define an appropriate measure for the entropy production we note that we can rewrite Equation (2.103) in the following way

$$\Sigma = \frac{1}{2T} \int dt\, dx\, \left\langle \partial_t \phi(x,t) F^{\text{ext}}(t) \right\rangle = \frac{L^d}{2T} \int dt\, \left\langle \partial_t m F^{\text{ext}}(t) \right\rangle \tag{3.10}$$

such that we integrate out the internal degrees of freedom of the order parameter field, ϕ. This has the practical advantage of eliminating the need to store complete field configurations when computing entropy production trajectories.

3.2.1 Estimation of Equilibrium Critical Exponents

To obtain the static critical exponents: α, β, γ and ν, the field has to be evolved for a sufficiently long time so that it reaches an equilibrium or at least a near equilibrium configuration. Consequently, the field is evolved to $t = 10^5$, where statistics are collected at every time unit. The evolution of the field for three different temperatures is exemplified in Figure 3.2. Moreover, the first 15000 data points are regarded as burn-in and are thus discarded. To get reliable statistics, the relevant quantities are averaged over 10 independently initialized runs. These simulations are done for 2D and 3D fields with side lengths $L = 8, 16, 32, 64$, to enable a finite-size scaling analysis. To extract critical exponents, a curve is fitted to a log-log plot of the relevant thermodynamic quantities using the `curve_fit` function from the `scipy.optimize` library [42].

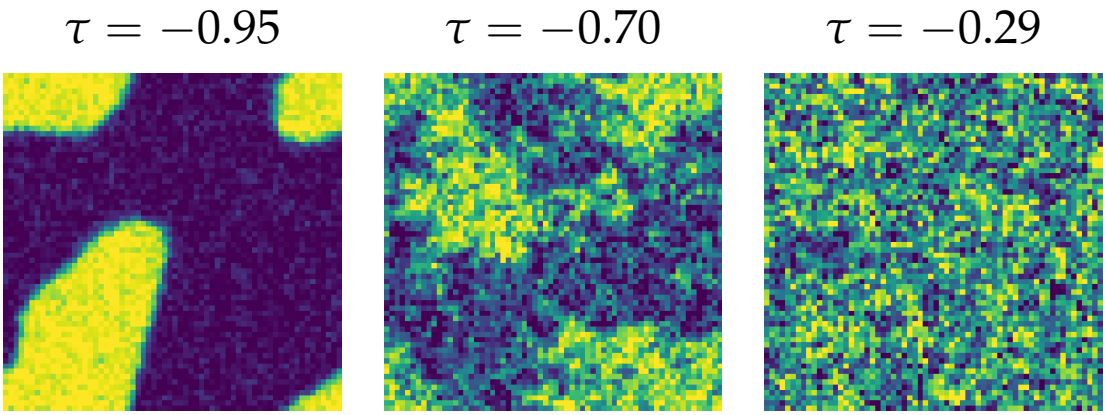

Figure 3.2: Snapshot of 2D, $L = 64$ fields under TDGL dynamics at $t = 100$ at three different temperatures.

3.2.2 Beyond Equilibrium

To emulate an incident laser pulse, we will set the external field to

$$F^{\text{ext}}(t) = h_0 \sin(\omega t), \tag{3.11}$$

i.e. a spatially homogeneous sinusoidal field. The approximation that the field has no spatial variation is well founded – since the diameter of the laser pulse in ultrafast spectroscopy experiments often is much larger than the sample size. While previous theoretical studies have modeled the laser field as a gaussian wavepacket [8, 9], our choice of a purely sinusoidal field is a simplification that serves as a first step to understanding the dynamics of ultrafast magnetization. The protocol for the laser is defined as the following: The field is initialized to a random configuration and then evolved freely, without an external field, from $t = 0$ to $t = 100$. Subsequently, external field is turned on and then drives the order parameter field from $t = 100$ to $t = 1100$, wherein data is collected. This process is then averaged over 500 separate initializations, for each value of τ.

4

Results

This chapter is divided into two parts. The first part, Section 4.1, covers the extraction of critical exponents of equilibrium thermodynamic quantities. The second part, Section 4.2, details the analytical derivation of a closed-form expression for the entropy production. The validity of this expression is then assessed by comparing it to numerical simulations of the entropy production.

4.1 Equilibrium

This section contains the finite-size scaling analysis of the magnetization, magnetic susceptibility, and heat capacity for 2D and 3D scalar order parameter fields with TDGL dynamics. In addition, the Binder cumulant is calculated to ascertain the critical point and the value of the critical exponent ν. Established values of the critical exponents – along with values calculated in this work are compiled and compared in Table 4.1.

4.1.1 Binder Cumulant

Figure 4.1a and Figure 4.2a show Binder cumulants obtained from TDGL simulations for 2D and 3D systems of varying sizes. From these figures, we can obtain an estimate for the effective critical point τ_C, by extracting the point of intersection of the Binder cumulants of the largest ($L = 64$) and the second largest system ($L = 32$). These effective critical points were $\tau_C = -0.6844$ for the 2D system, and $\tau_C = -0.5265$ for the 3D system. By shifting and rescaling the x-axis $\tau \to (\tau - \tau_C)L^{1/\nu}$ we see in Figure 4.1b and Figure 4.2b that the Binder cumulants for all system sizes collapse onto a single line. This is an indication that the effective critical points were chosen correctly and that the known values for the critical exponent ν ($\nu = 1$ and $\nu = 0.63$ for 2D and 3D respectively) are in agreement with the data obtained from the simulations.

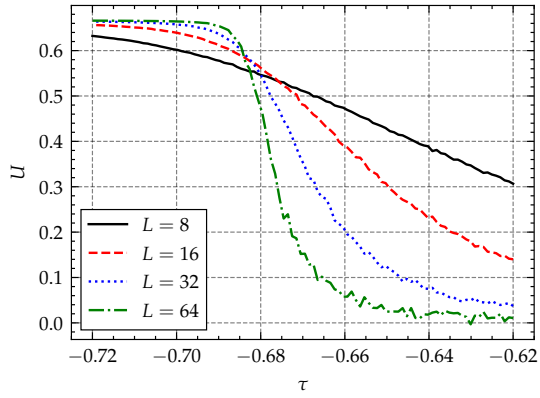

(a) Binder cumulants for different system sizes.

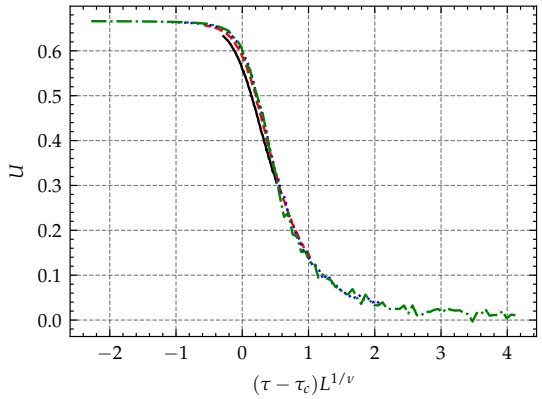

(b) Binder cumulants collapsed onto a single curve by choosing $\nu = 1$ and $\tau_C = -0.6844$

Figure 4.1: Finite-size scaling of the Binder cumulant in 2D.

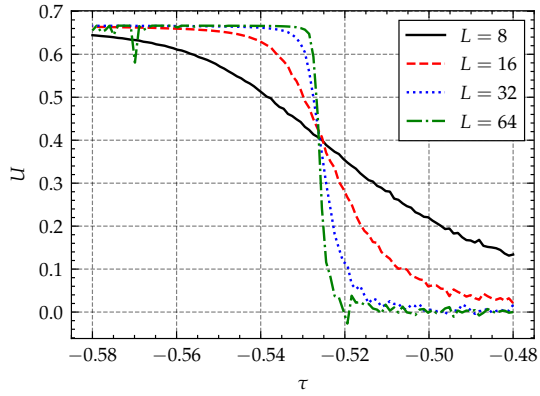

(a) Binder cumulants for different system sizes.

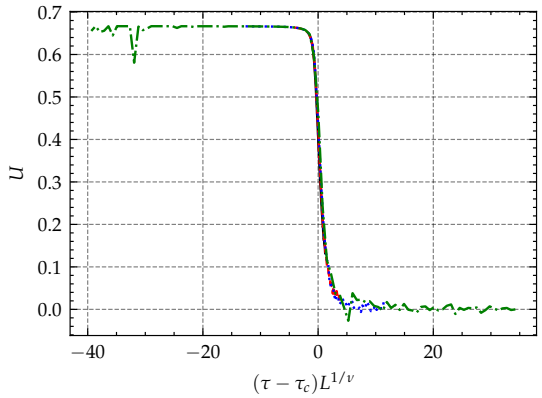

(b) Binder cummulants collasped unto a single curve by choosing $\nu = 0.63$ and $\tau_C = -0.5265$

Figure 4.2: Finite-size scaling of the Binder cumulant in 3D.

4.1.2 Magnetization

Figure 4.3a and Figure 4.4a show the magnetization $|M|$, plotted against the control parameter τ for a 2D and a 3D system, respectively. For both the 2D and the 3D systems, the finite-size effects are striking. For systems with a side length of $L = 8$, the magnetization is almost monotonic, and no distinct phase transition is apparent. On the contrary, for a system with a side length of $L = 64$, we can see a pronounced phase transition that separates the ordered and the disordered phase. In Figure 4.3b and Figure 4.4b the value of the magnetization at the effective critical point is plotted against system size in a log-log plot. The slope of the fitted line is equal to the negative ratio of the critical exponents β and ν. As such, we get that $\frac{\beta}{\nu} = 0.1234$ for the 2D system and $\frac{\beta}{\nu} = 0.5499$ for

the 3D systems, and the deviation from the known values ($\frac{\beta}{\nu} = \frac{1}{8} = 0.125$ for 2D and $\frac{\beta}{\nu} = 0.518$ for 3D) are 1.28% and 6.16% for 2D and 3D, clearly showing that the simulations exhibit a qualitative and, to some degre,e quantitative agreement with known results.

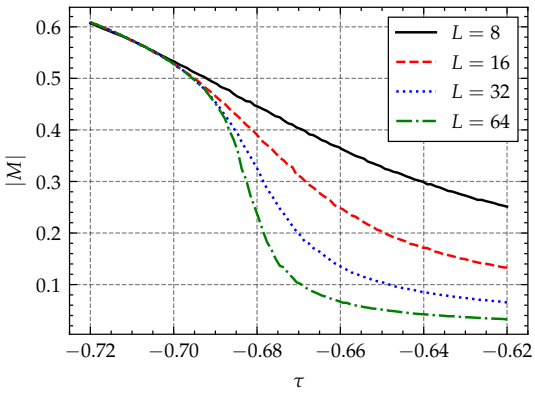

(a) Plot of the magnetization $|M|$, against the controll parameter τ, for different values of the system size L.

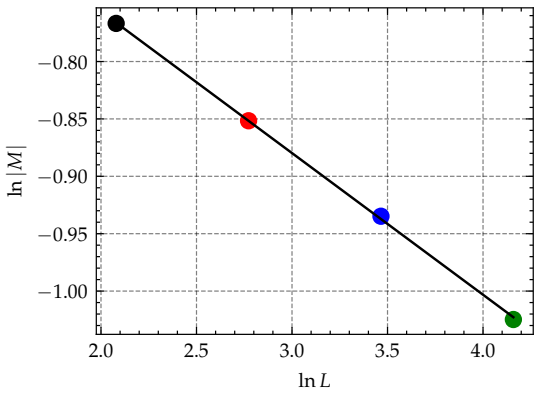

(b) Log-log plot of the magnetization $|M|$, at the critical point plotted against the system size L. The solid black line shows the logarithm of an exponential function that is fitted to the data.

Figure 4.3: Finite-size scaling of the magnetization in 2D.

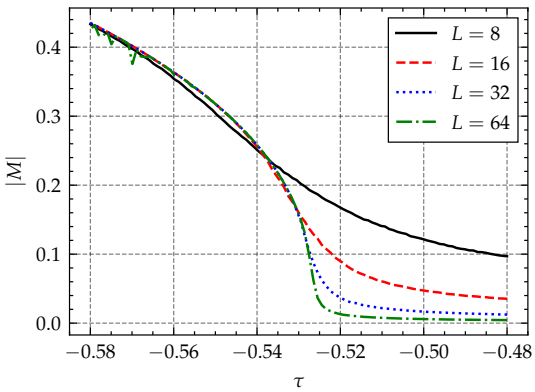

(a) Plot of the magnetization $|M|$, against the controll parameter τ, for different values of the system size L.

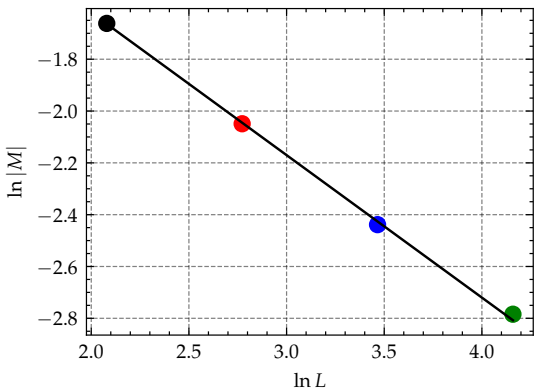

(b) Log-log plot of the magnetization $|M|$, at the critical point plotted against the system size L. The solid black line shows the logarithm of an exponential function that is fitted to the data.

Figure 4.4: Finite-size scaling of the magnetization in 3D.

4.1.3 Susceptibility

Figure 4.5a and Figure 4.6a show the magnetic susceptibility $\chi_{|M|}$ plotted against the control parameter τ. From these plots we see that the divergent tendency of the magnetic susceptibility is only really apparent for the systems with a side length of $L = 64$. For smaller systems finite-size effects inhibit the singularity in susceptibility we expect at τ_C. In Figure 4.5b and Figure 4.6b the value of the magnetic susceptibility at the critical point is plotted against system size, for 2D and 3D systems, in a log-log plot. Once again, the slope of the fitted curves reveals the critical exponent ratios. They are $\gamma/\nu = 1.5916$ for the 2D system and $\gamma/\nu = 1.8511$ for the 3D system. This is a deviation of 9.1% and 5.7% from the established critical exponent ratios of $\gamma/\nu = 7/4 = 1.75$ and γ/ν=1.964 for 2D and 3D systems. Again, this shows that qualitatively the critical scaling of the magnetic susceptibility has been captured to some extent.

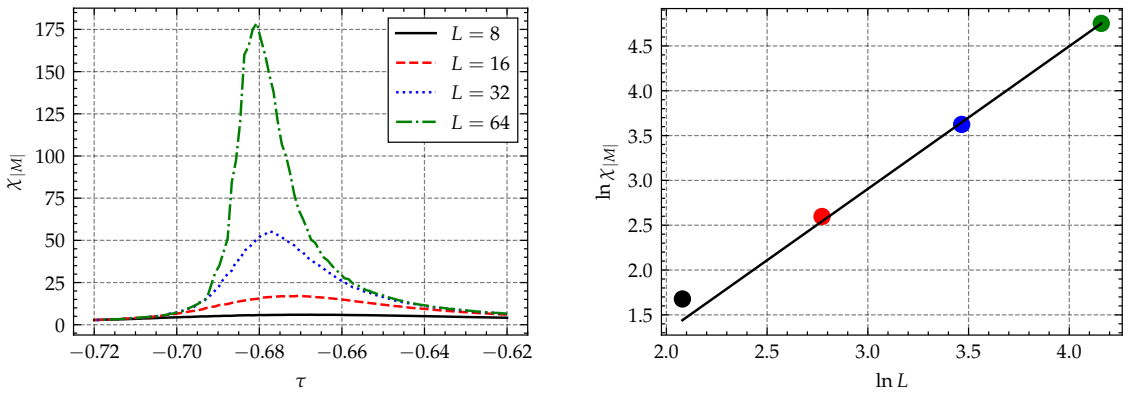

(a) Plot of the magnetic susceptibility $\chi_{|M|}$, against the control parameter τ, for different values of the system size L.

(b) Log-log plot of the magnetic susceptibility $\chi_{|M|}$, at the critical point plotted against the system size L. The solid black line shows the logarithm of an exponential function that is fitted to the data.

Figure 4.5: Finite-size scaling of the magnetic susceptibility in 2D.

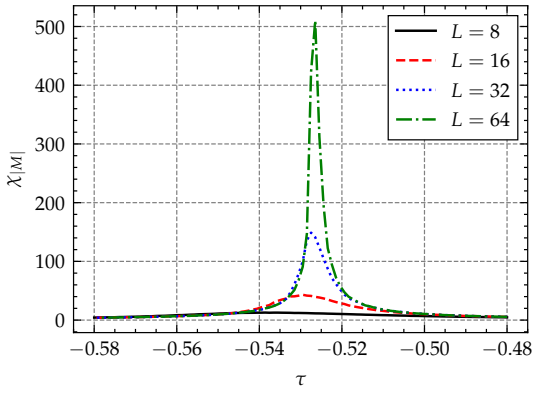

(a) Plot of the magnetic susceptibility $\chi_{|M|}$, against the control parameter τ, for different values of the system size L.

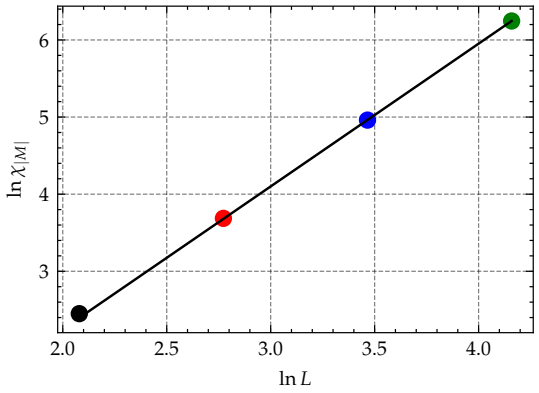

(b) Log-log plot of the magnetic susceptibility $\chi_{|M|}$, at the critical point plotted against the system size L. The solid black line shows the logarithm of an exponential function that is fitted to the data.

Figure 4.6: Finite-size scaling of the magnetic susceptibility in 3D.

4.1.4 Heat Capacity

Figure 4.7a and Figure 4.8a show the heat capacity C, plotted against the control parameter τ. In 2D, the heat capacity is only logarithmically divergent, which is evident from Figure 4.7b where the value of the heat capacity is plotted against system size. Here we see that a logarithmic curve is successfully fitted to the data points. In 3D, the heat capacity is, however, divergent. From Figure 4.8b, where the value of the heat capacity at the critical point is plotted against the system size in a log-log plot, we obtain that the associated critical exponent ratio is $\alpha/\nu = 0.2010$. This is a deviation of 14.9% from the true value of $\alpha/\nu = 0.175$. Even though the discrepancy is notable, the fact that the 3D system exhibits a power law divergence whilst the 2D system is logarithmically divergent is indicative that the method used qualitatively captures the critical scaling of the heat capacity.

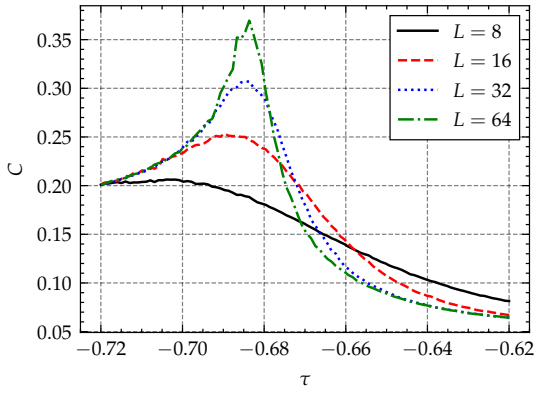

(a) Plot of the heat capacity C, against the control parameter τ, for different values of the system size L.

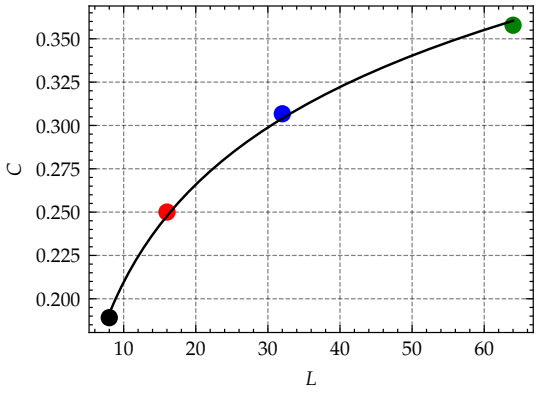

(b) Plot of the heat capacity C, at the critical point plotted against the system size L. The solid black line shows a logarithmic function that is fitted to the data.

Figure 4.7: Finite-size scaling of the heat capacity in 2D.

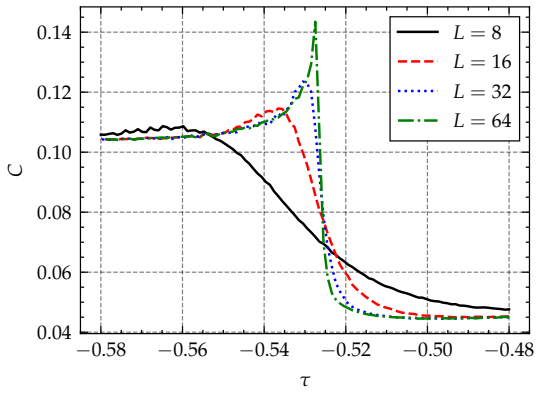

(a) plot of the heat capacity C, against the control parameter τ, for different values of the system size L.

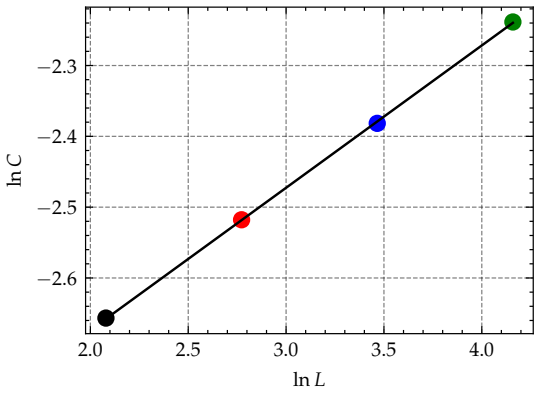

(b) Log-log plot of the heat capacity C, at the critical point plotted against the system size L. The solid black line shows the logarithm of an exponential function that is fitted to the data.

Figure 4.8: Finite-size scaling of the heat capacity in 3D.

4.1.5 Brief Summary

Table 4.1 summarizes all critical exponent ratios that were obtained from the finite-size scaling analysis in the previous subsections. As stated previously, these results clearly show that TDGL simulations are exhibiting a critical scaling behaviour that is qualitatively correct: The critical exponent ratios are consistently larger in 3D than in 2D; the heat capacity diverges logarithmically in 2D and with a power law in 3D.

Table 4.1: Critical exponent ratios for 2D and 3D systems obtained in this work compared to known values. Known 2D values are obtained analytically from the Onsager solution, known 3D values are obtained from state-of-the art numerical Monte Carlo simulations. "0" indicates that a logarithmic function was successfully fitted to the data.

		α/ν	β/ν	γ/ν
Known values	3D [43]	0.175	0.518	1.964
	2D [19]	0	1/8	7/4
Present work	3D	0.2010	0.5499	1.8511
	2D	"0"	0.1234	1.5916

To ascertain whether systematic errors are present, we may check if the scaling laws/critical exponent identities introduced in Section 2.1.5 hold for our numerically obtained critical exponents. In 2D, Josephson's Identity ($2 - \alpha = \nu d$) is trivially satisfied, and in 3D (where $\nu = 0.63$) we get an approximate agreement

$$0.63(3 + 0.2010) = 2.0223, \tag{4.1}$$

with a deviation of 1.12%. Furthermore, in 2D, Rushbrooke's Identity ($\alpha + 2\beta + \gamma = 2$)

$$0 + 2 \cdot 0.1234 + 1.5916 = 1.8384 \tag{4.2}$$

holds to a lesser degree, deviating 8.3%, while in 3D

$$0.63(0.2010 + 2 \cdot 0.5499 + 1.8511) = 1.9857 \tag{4.3}$$

the agreement is stronger, only deviating 0.72%. As such, we can hypothesize that there exists some internal consistency of errors for at least the 3D simulations, since the deviations from the scaling laws are lower than the deviations from the individual critical exponents.

4.2 Out of equilibrium

This section covers first the analytical derivation of a closed-form expression of the entropy production of a scalar order parameter field coupled to an external sinusoidal drive. This expression is then compared to numerical data – and its validity is assessed.

4.2.1 Response of the Field

Under the influence of an external oscillating field, we may hypothesize that the order parameter will oscillate as well

$$\phi(x, t) = m_0 + \phi_0 \sin(\omega t + \varphi), \tag{4.4}$$

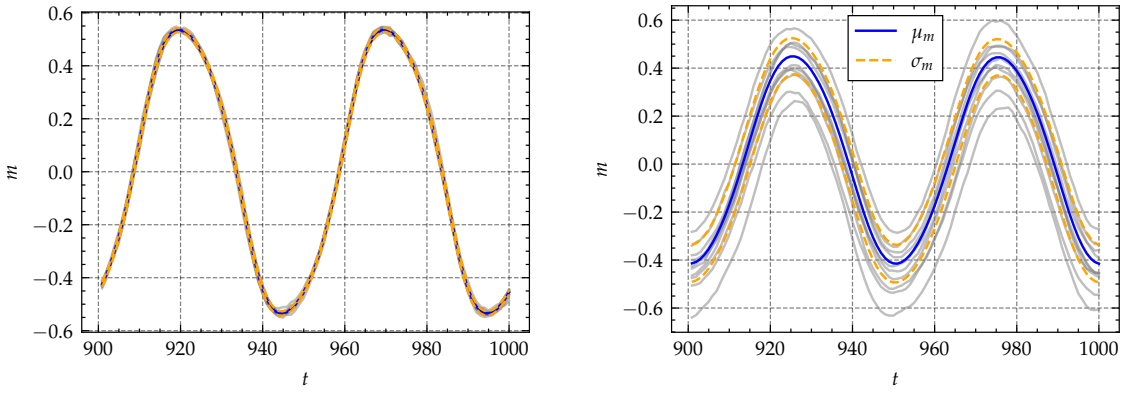

(a) Magnetization trajectory in the disordered phase, for $\tau = -0.61$.

(b) Magnetization trajectory in the ordered phase, for $\tau = -0.75$.

Figure 4.9: Plot of the instantaneous magnetization m against time t, for a 2D, $L = 64$ field driven by an external field with $\omega = 0.04\pi$ and $h_0 = 0.1$. The mean over trajectories is plotted in blue and $\pm 1\sigma$ in orange. A number of individual trajectories in grey are also included.

around some fixed value m_0 with an amplitude ϕ_0. This assumption is in part phenomenological. In Figure 4.9 we see that under a harmonic drive, the instantaneous magnetization oscillates more or less sinusoidally. Furthermore, we posit that the response of the order parameter field lags behind the driving laser, thereby incurring a phase shift φ. If we take this expression and insert it into the TDGL equation we get

$$\phi_0\omega\cos(\omega t+\varphi) = -2\gamma\alpha\tau\phi_0\sin(\omega t+\varphi) + \gamma h_0\sin(\omega t) + \eta(x,t) - 2\gamma\alpha\tau m_0, \quad (4.5)$$

where we have neglected higher-order terms under the assumption that we are near the critical point and ϕ is small. Moreover, to explicitly study how the phase shift, φ, depends on the driving frequency of the laser ω, we may disregard the last two terms. As such we are left with

$$\phi_0\omega\cos(\omega t+\varphi) = -2\gamma\alpha\tau\phi_0\sin(\omega t+\varphi) + \gamma h_0\sin(\omega t). \quad (4.6)$$

To proceed we will shift the time $\omega t \to \omega t - \varphi$ and rewrite the shifted field as $\sin(\omega t-\varphi) = \sin(\omega t)\cos(\varphi) - \cos(\omega t)\sin(\varphi)$. After rearranging the terms we get

$$\cos(\omega t)\left(\phi_0\omega + \gamma h_0\sin(\varphi)\right) = \sin(\omega t)\left(\gamma h_0\cos(\varphi) - 2\gamma\alpha\tau\phi_0\right). \quad (4.7)$$

If the equation above is to hold for all t, we need

$$\sin(\varphi) = -\frac{\phi_0\omega}{\gamma h_0}, \quad \cos(\varphi) = \frac{2\alpha\tau\phi_0}{h_0}. \quad (4.8)$$

Combining these results we get

$$\tan(\varphi) = -\frac{\omega}{2\alpha\tau\gamma} \implies \varphi = -\arctan\left(\frac{\omega}{2\alpha\tau\gamma}\right). \quad (4.9)$$

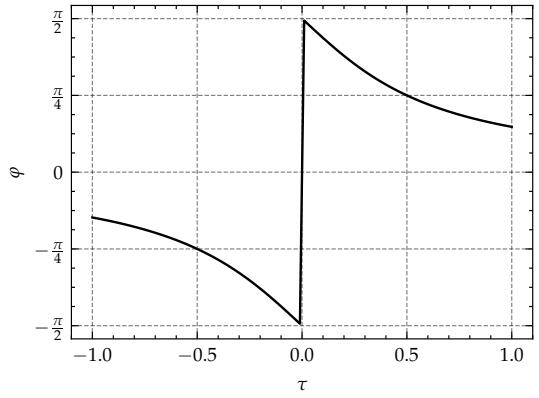

(a) Plot of the phase shift between the laser field and the response field, φ against the control parameter τ, for $\omega/\alpha\gamma = 1$.

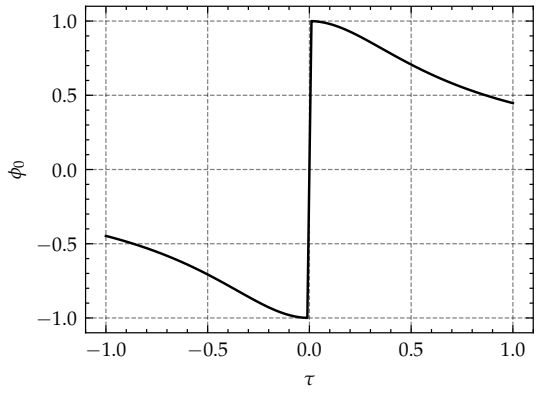

(b) Plot of the amplitude of the response field, ϕ_0 against the control parameter τ, for $\omega/\alpha\gamma = 1$ and $h_0/\alpha = 1$.

Figure 4.10: Analytic expressions for the amplitude, ϕ_0, and the phase shift, φ of the response field.

Using Equation (4.8) and Equation (4.9) we may also extract an expression for the amplitude of the response field

$$\phi_0 = \frac{h_0}{2\alpha\tau}\cos(\varphi) = \frac{h_0}{2\alpha\tau}\frac{1}{\sqrt{1+\left(\frac{\omega}{2\alpha\tau\gamma}\right)^2}}. \tag{4.10}$$

4.2.2 Analytical Expression for Entropy Production

Now that we have an ansatz for the response of the field to the external field we may derive a closed form expression for the entropy production.

$$\Sigma = \frac{1}{2T}\int dx\,dt\,\left\langle \partial_t\phi(x,t)F^{\text{ext}}(t)\right\rangle = \frac{L^d}{2T}\int dt\,\phi_0\omega\cos(\omega t+\varphi)h_0\sin(\omega t), \tag{4.11}$$

Since we are working with a periodic drive we may set the bounds of integration to be one period of the laser field, $t \in [0, 2\pi/\omega]$. Furthermore we now define an intensive expression for the entropy production $\widetilde{\Sigma} \equiv \frac{1}{L^d}\frac{\omega}{2\pi}\Sigma$. Evaluating the integral now gives us

$$\widetilde{\Sigma} = \frac{1}{2T}\frac{\omega h_0\phi_0}{2}\sin(\varphi). \tag{4.12}$$

We may set $\sin(\varphi) = \sqrt{\frac{\tan^2(\varphi)}{1+\tan^2(\varphi)}}$, if we also set $\phi_0 = h_0/\sqrt{(2\alpha\tau)^2+(\omega/\gamma)^2}$. Using Equation (4.9) we arrive at

$$\widetilde{\Sigma} = \frac{1}{2T}\frac{\gamma h_0^2}{2}\frac{\omega^2}{(2\alpha\tau\gamma)^2+\omega^2}, \tag{4.13}$$

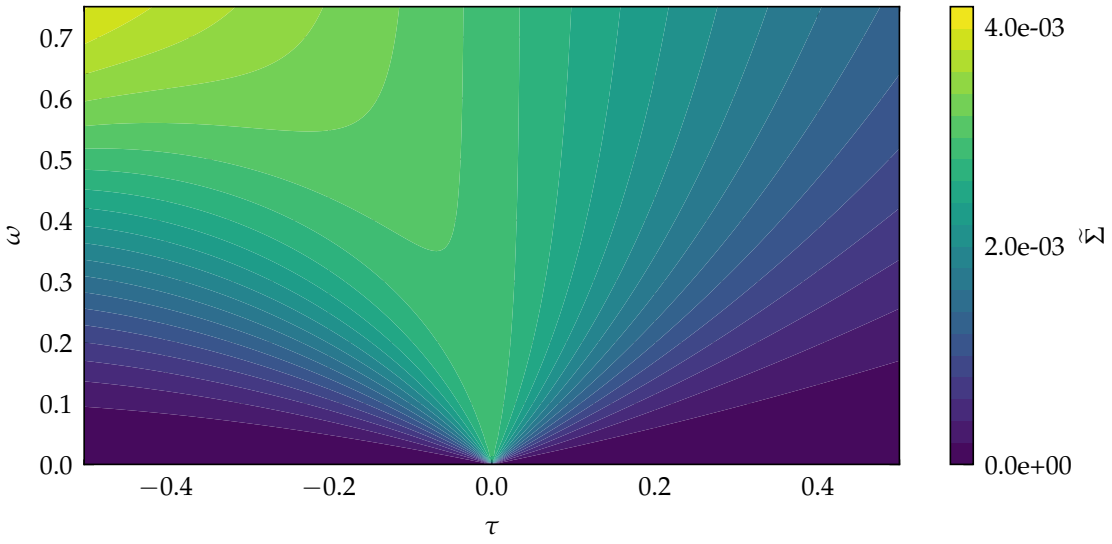

Figure 4.11: Entropy production as a function of the driving frequency ω and the control parameter τ.

which constitutes one main result of this thesis. The (intensive) *dissipated heat*, which is defined as $w \equiv T\widetilde{\Sigma}$, is thus a Lorentzian centered at the critical point. In the high drive frequency limit we note that the entropy production becomes inversely proportional to the temperature

$$\widetilde{\Sigma} \xrightarrow[\omega\to\infty]{} \frac{1}{2T}\frac{\gamma h_0^2}{2}. \tag{4.14}$$

Conversely, in the low drive frequency limit we expect the entropy production to peak at the critical point $\tau = 0$, albeit with a vanishing amplitude

$$\widetilde{\Sigma} \xrightarrow[\omega\to 0]{} \frac{1}{2T}\frac{\gamma h_0^2 \omega^2}{(2\alpha\tau\gamma)^2} \to 0, \tag{4.15}$$

which keeps it from diverging properly, as seen in Figure 4.11. Consequently, since the entropy production does not diverge at the critical point, we do not expect the entropy production to exhibit any finite-size scaling. Moreover, since the entropy production is analytic at all points $T \neq 0$, we do not expect the derivative of the entropy production with respect to τ, $\partial_\tau \widetilde{\Sigma}$, to scale either.

4.2.3 Comparison to Numerical Results

Figure 4.12 shows the entropy production obtained from TDGL simulations besides the entropy production computed analytically from Equation (4.13), where the inclusion of noise is accounted for by the shift $\tau \to \tau - \tau_C$. Some differences are noticeable. In the ordered phase, for small τ, the analytical expression overestimates the entropy production greatly. Moreover, in Figure 4.12a we see that the peak of the entropy production shifts towards the ordered phase for lower driving frequencies – away from the equilibrium critical point $\tau_C = -0.6844$,

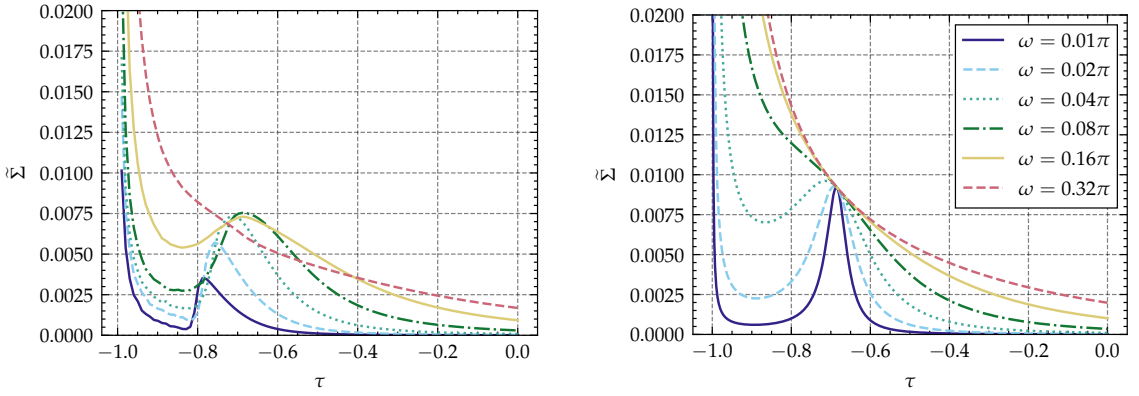

(a) Numerical simulations of entropy production plotted against the control parameter τ.

(b) Analytically calculated entropy production plotted against the control parameter τ.

Figure 4.12: Comparison of Equation (4.13) with numerically computed entropy production for a 2D, $L = 64$ field, for a few different driving frequencies and a driving amplitude $h_0 = 0.1$.

and that the amplitude of the peak decreases sharply – these are features that are not recreated in the analytic expression. Despite these significant inconsistencies, there seems to be some merit to the expression – we see in Figure 4.13a, Figure 4.14a and Figure 4.15a that in the frequency regime $\omega = 0.04\pi - 0.16\pi$, Equation (4.13) accurately reproduces the numerical entropy production in the disordered phase. To emphasize this agreement, in Figure 4.13b, Figure 4.14b and Figure 4.15b the dissipated heat is plotted, to show that the entropy production does not trivially reproduce $\widetilde{\Sigma} \propto 1/T$. That the analytical expression is more valid in the disordered phase should be expected – the linearization of the TDGL equation assumes that the value of the order parameter is low so that we can neglect higher order terms.

That the entropy production shifts towards the ordered phase as the driving frequency decreases should not be altogether surprising either. Suppose that the ϕ^3-term is included in the ansatz for the response of the field and that higher order harmonics are neglected. Then the peak of the phase shift will become offset towards the ordered phase

$$\varphi \approx -\arctan\left(\frac{\omega}{2\alpha\tau + 3\beta\phi_0^2}\right). \tag{4.16}$$

Moreover, in the linearized approximation the field amplitude is inversely proportional to the driving frequency $\phi_0 \sim 1/\omega$, and as such this offset would become more pronounced for lower values of ω. This much simplified analysis of the consequences of the inclusion of the cubic term does not, however, explain why the entropy production decreases altogether for lower values of ω, and rigorous calculations would be needed to definitively ascertain the role of higher order terms.

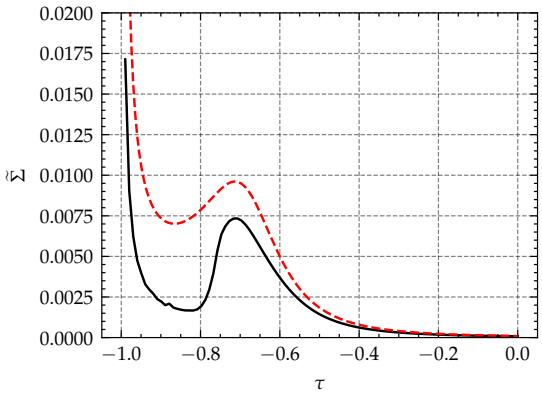

(a) Numerical simulation and analytical calculation of entropy production plotted against the control parameter τ.

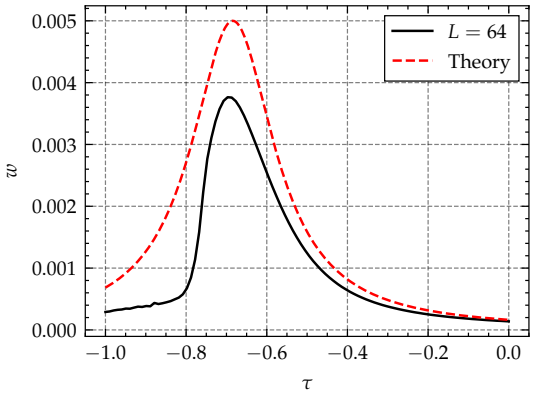

(b) Numerical simulation and analytical calculation of dissipated heat plotted against the control parameter τ

Figure 4.13: Comparison between analytical and numerical results for a 2D, $L = 64$ field with a driving frequency and amplitude of $\omega = 0.04\pi$ and $h_0 = 0.1$.

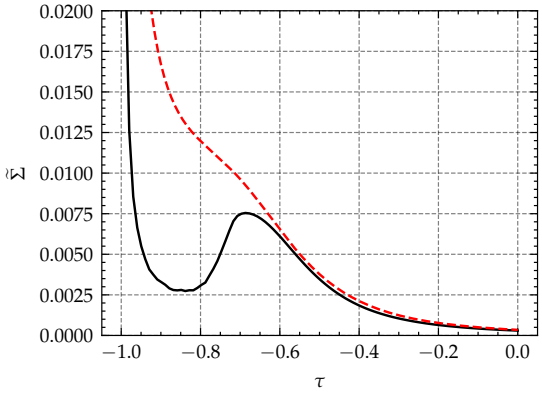

(a) Numerical simulation and analytical calculation of entropy production plotted against the control parameter τ.

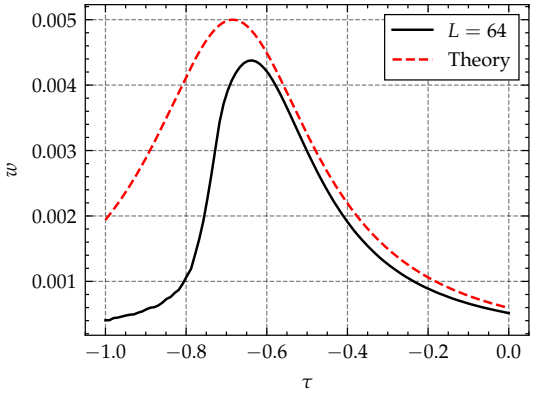

(b) Numerical simulation and analytical calculation of dissipated heat plotted against the control parameter τ.

Figure 4.14: Comparison between analytical and numerical results for a 2D, $L = 64$ field with a driving frequency and amplitude of $\omega = 0.08\pi$ and $h_0 = 0.1$.

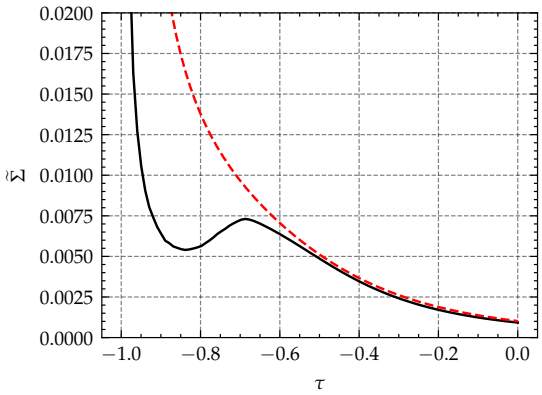

(a) Numerical simulation and analytical calculation of entropy production plotted against the control parameter τ.

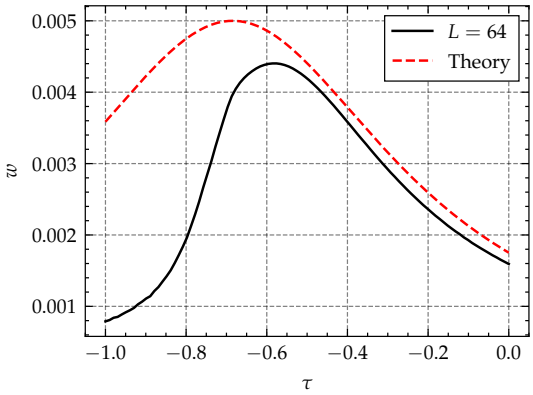

(b) Numerical simulation and analytical calculation of dissipated heat plotted against the control parameter τ.

Figure 4.15: Comparison between analytical and numerical results for a 2D, $L = 64$ field with a driving frequency and amplitude of $\omega = 0.16\pi$ and $h_0 = 0.1$.

4.2.4 Finite-size Scaling of Entropy Production

In this subsection, a finite-size scaling analysis of the entropy production for a 2D field with a harmonic drive of amplitude $h_0 = 0.1$ and frequency $\omega = 0.04\pi$ is presented. From Figure 4.16 we see once again that the entropy production is not cusped at the equilibrium critical point. Furthermore, the entropy production computed for different system sizes seems to converge to one smooth function. This is consistent with the prediction in Subsection 4.2.2 that the entropy production should not diverge at the critical point and, as such, will not exhibit critical scaling or substantial finite-size effects at the critical point.

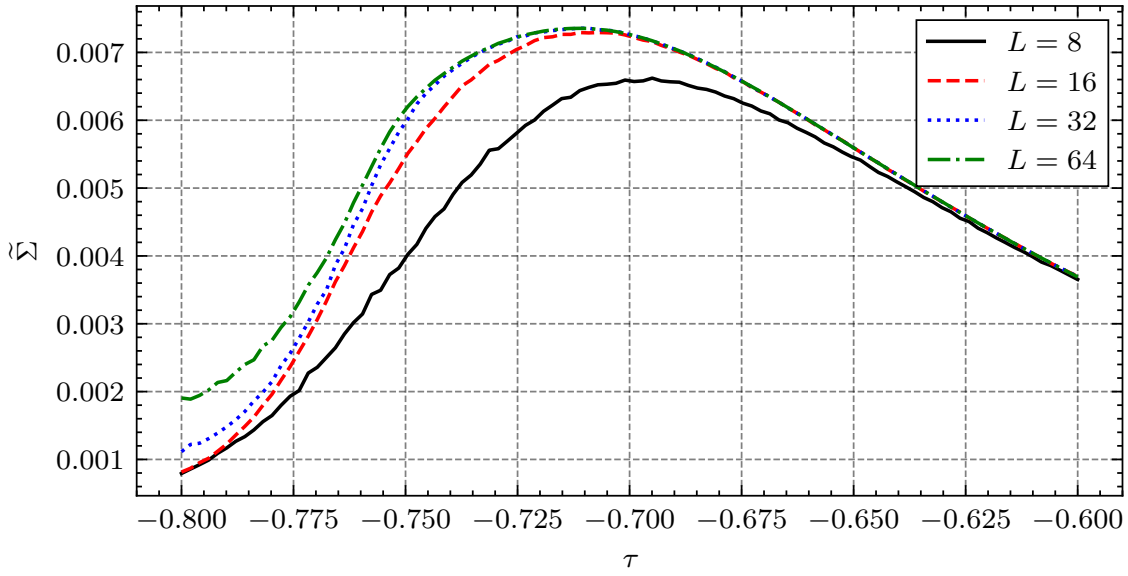

Figure 4.16: Finite-size scaling of the entropy production for a 2D field. The amplitude and frequency of the driving field were $h_0 = 0.1$ and $\omega = 0.04\pi$

5
Conclusion

This thesis has studied the entropy production of a scalar order parameter field coupled to an external time-dependent sinusoidal field. Furthermore, the method of using the time-dependent Ginzburg-Landau equation to govern the dynamics of the field was validated through the extraction of equilibrium critical exponents. Comparison between known critical exponents and those obtained in this work showed a clear qualitative and quantitative agreement, to such an extent that one can be confident that the model reproduces the expected universal critical behavior in the equilibrium limit. It should, however, be emphasized that if the only goal of this thesis was to extract equilibrium critical exponents with as high a degree of numerical accuracy as possible, then there are likely methods that are more suitable than the TDGL approach. These include state-of-the-art hardware-accelerated Monte Carlo algorithms [44], as well as methods that build upon theoretical frameworks such as the conformal bootstrap [45].

Furthermore, the entropy production of the scalar order parameter field coupled to a spatially homogeneous sinusoidal drive was computed. A finite-size scaling analysis shows that the entropy production converges to a smooth function around the critical point for a driving field with frequency $\omega = 0.04\pi$ and amplitude $h_0 = 0.1$. It should be emphasized that this assessment is valid only for this particular drive protocol and the possibility that the entropy production has a distinct critical behavior for other driving fields should not be ruled out.

An analytical expression for the entropy production is proposed, which shows a quantitative agreement with simulations in the disordered phase for a driving amplitude of $h_0 = 0.1$ and driving frequencies in the range $\omega = 0.04\pi - 0.16\pi$. The peak of the entropy production is offset towards the ordered phase, and this offset increases for lower driving frequencies – something which is not reproduced in the analytical expression. It is hypothesized that this discrepancy is due to the neglect of higher order terms in the TDGL equation. As such, the incorporation of higher order terms could be a suitable starting point for further studies on the topic. Moreover, an ansatz that takes into account the spatial variation of the order parameter field could also be a promising direction of research.

In this work, the driving amplitude has been kept constant. However, a parameter scan over different combinations of driving frequency and amplitude is likely needed to reach a comprehensive understanding of the entropy production of a harmonically driven order parameter field. This has not been undertaken in

this thesis primarily due to time constraints. Looking ahead, to be able to make any quantitative predictions about the outcome of experiments, it would be necessary to move beyond the sinusoidal driving field and explore more realistic waveforms.

It also ought to be mentioned that statistical field theory and critical phenomena are deeply connected to the concept of the *renormalization group*. To review and incorporate this theoretical framework has been deemed beyond the scope of this thesis, but it would be a natural starting point for any future work that aims to take a more theoretical approach to the subject.

To conclude, this work has taken initial steps towards incorporating critical phenomena in ultrafast thermodynamics. A method of simulation for this purpose – the TDGL equation – is validated. Under a simplified driving field, the system exhibits a smooth, but non-trivial entropy production, which in part can be explained analytically.

Bibliography

[1] M. Maiuri, M. Garavelli, and G. Cerullo, "Ultrafast spectroscopy: State of the art and open challenges," *Journal of the American Chemical Society*, vol. 142, no. 1, pp. 3–15, 2020, PMID: 31800225. DOI: 10.1021/jacs.9b10533. eprint: https://doi.org/10.1021/jacs.9b10533. [Online]. Available: https://doi.org/10.1021/jacs.9b10533.

[2] L. Poisson and F. Lépine, "Ultrafast phenomena from attosecond to picosecond timescales: Theory and experiments," *The European Physical Journal Special Topics*, vol. 232, no. 13, pp. 1995–2000, Sep. 2023.

[3] M. Budden *et al.*, "Evidence for metastable photo-induced superconductivity in k3c60," *Nature Physics*, vol. 17, no. 5, pp. 611–618, Feb. 2021, ISSN: 1745-2481. DOI: 10.1038/s41567-020-01148-1. [Online]. Available: http://dx.doi.org/10.1038/s41567-020-01148-1.

[4] J. W. McIver *et al.*, "Light-induced anomalous hall effect in graphene," *Nature Physics*, vol. 16, no. 1, pp. 38–41, Nov. 2019, ISSN: 1745-2481. DOI: 10.1038/s41567-019-0698-y. [Online]. Available: http://dx.doi.org/10.1038/s41567-019-0698-y.

[5] J. Igarashi *et al.*, "Optically induced ultrafast magnetization switching in ferromagnetic spin valves," *Nature Materials*, vol. 22, pp. 1–6, Mar. 2023. DOI: 10.1038/s41563-023-01499-z.

[6] A. de la Torre, D. M. Kennes, M. Claassen, S. Gerber, J. W. McIver, and M. A. Sentef, "Colloquium: Nonthermal pathways to ultrafast control in quantum materials," *Reviews of Modern Physics*, vol. 93, no. 4, Oct. 2021, ISSN: 1539-0756. DOI: 10.1103/revmodphys.93.041002. [Online]. Available: http://dx.doi.org/10.1103/RevModPhys.93.041002.

[7] U. Seifert, "Stochastic thermodynamics: Principles and perspectives," *The European Physical Journal B*, vol. 64, no. 34, pp. 423–431, Jan. 2008, ISSN: 1434-6036. DOI: 10.1140/epjb/e2008-00001-9. [Online]. Available: http://dx.doi.org/10.1140/epjb/e2008-00001-9.

[8] L. Caprini, H. Löwen, and R. M. Geilhufe, *Ultrafast entropy production in pump-probe experiments*, 2023. arXiv: 2302.02716 [cond-mat.mtrl-sci]. [Online]. Available: https://arxiv.org/abs/2302.02716.

[9] F. Tietjen and R. M. Geilhufe, "Ultrafast entropy production in nonequilibrium magnets," *PNAS Nexus*, vol. 4, no. 3, P. Sharma, Ed., Feb. 2025, ISSN: 2752-6542. DOI: 10.1093/pnasnexus/pgaf055. [Online]. Available: http://dx.doi.org/10.1093/pnasnexus/pgaf055.

[10] J. Walowski and M. Munzenberg, "Perspective: Ultrafast magnetism and thz spintronics," *Journal of Applied Physics*, vol. 120, no. 14, p. 140 901, Aug. 2016, ISSN: 0021-8979. DOI: 10.1063/1.4958846. eprint: https://pubs.aip.org/aip/jap/article-pdf/doi10.1063/1.4958846/19952803/140901_1_1.4958846.pdf. [Online]. Available: https://doi.org/10.1063/1.4958846.

[11] R. G. Endres, *Entropy production selects nonequilibrium states in multistable systems*, 2017. arXiv: 1710.02600 [q-bio.QM]. [Online]. Available: https://arxiv.org/abs/1710.02600.

[12] C. Nardini, É. Fodor, E. Tjhung, F. van Wijland, J. Tailleur, and M. E. Cates, "Entropy production in field theories without time-reversal symmetry: Quantifying the non-equilibrium character of active matter," *Physical Review X*, vol. 7, no. 2, Apr. 2017, ISSN: 2160-3308. DOI: 10.1103/physrevx.7.021007. [Online]. Available: http://dx.doi.org/10.1103/PhysRevX.7.021007.

[13] I. F. Mello, L. Squillante, G. O. Gomes, A. C. Seridonio, and M. de Souza, "Epidemics, the ising-model and percolation theory: A comprehensive review focused on covid-19," *Physica A: Statistical Mechanics and its Applications*, vol. 573, p. 125 963, Jul. 2021, ISSN: 0378-4371. DOI: 10.1016/j.physa.2021.125963. [Online]. Available: http://dx.doi.org/10.1016/j.physa.2021.125963.

[14] H. Suzuki, J.-i. Imura, and K. Aihara, "Chaotic ising-like dynamics in traffic signals," *Scientific reports*, vol. 3, p. 1127, Jan. 2013. DOI: 10.1038/srep01127.

[15] D. Stauffer, "Social applications of two-dimensional ising models," *American Journal of Physics*, vol. 76, no. 4, pp. 470–473, Apr. 2008, ISSN: 1943-2909. DOI: 10.1119/1.2779882. [Online]. Available: http://dx.doi.org/10.1119/1.2779882.

[16] E. Ising, "Beitrag zur Theorie des Ferromagnetismus," *Zeitschrift fur Physik*, vol. 31, no. 1, pp. 253–258, Feb. 1925. DOI: 10.1007/BF02980577.

[17] L. Onsager, "Crystal statistics. i. a two-dimensional model with an order-disorder transition," *Phys. Rev.*, vol. 65, pp. 117–149, 3-4 Feb. 1944. DOI: 10.1103/PhysRev.65.117. [Online]. Available: https://link.aps.org/doi/10.1103/PhysRev.65.117.

[18] G. M. Viswanathan, M. A. G. Portillo, E. P. Raposo, and M. G. E. da Luz, "What does it take to solve the 3d ising model? minimal necessary conditions for a valid solution," *Entropy*, vol. 24, no. 11, p. 1665, Nov. 2022, ISSN: 1099-4300. DOI: 10.3390/e24111665. [Online]. Available: http://dx.doi.org/10.3390/e24111665.

[19] K. Huang, *Statistical Mechanics*, 2nd ed. John Wiley & Sons, 1987, ch. 16.

[20] B. Widom, "Equation of state in the neighborhood of the critical point," *The Journal of Chemical Physics*, vol. 43, no. 11, pp. 3898–3905, Dec. 1965, ISSN: 0021-9606. DOI: 10.1063/1.1696618. eprint: https://pubs.aip.org/aip/jcp/article-pdf/43/11/3898/18841919/3898_1_online.pdf. [Online]. Available: https://doi.org/10.1063/1.1696618.

[21] G. S. Rushbrooke, "On the thermodynamics of the critical region for the ising problem," *The Journal of Chemical Physics*, vol. 39, no. 3, pp. 842–843, Aug. 1963, ISSN: 0021-9606. DOI: 10.1063/1.1734338. eprint: https://pubs.aip.org/aip/jcp/article-pdf/39/3/842/18830463/842_2_online.pdf. [Online]. Available: https://doi.org/10.1063/1.1734338.

[22] B. Widom, "Degree of the critical isotherm," *The Journal of Chemical Physics*, vol. 41, no. 6, pp. 1633–1634, Sep. 1964, ISSN: 0021-9606. DOI: 10.1063/1.1726135. eprint: https://pubs.aip.org/aip/jcp/article-pdf/41/6/1633/18835147/1633_1_online.pdf. [Online]. Available: https://doi.org/10.1063/1.1726135.

[23] B. D. Josephson, "Inequality for the specific heat: Ii. application to critical phenomena," *Proceedings of the Physical Society*, vol. 92, no. 2, p. 276, Oct. 1967. DOI: 10.1088/0370-1328/92/2/302. [Online]. Available: https://dx.doi.org/10.1088/0370-1328/92/2/302.

[24] M. E. Fisher, "Rigorous inequalities for critical-point correlation exponents," *Phys. Rev.*, vol. 180, pp. 594–600, 2 Apr. 1969. DOI: 10.1103/PhysRev.180.594. [Online]. Available: https://link.aps.org/doi/10.1103/PhysRev.180.594.

[25] A. Altland and B. D. Simons, *Condensed Matter Field Theory*, 2nd ed. Cambridge University Press, 2010.

[26] R. Bowers, "The universality hypothesis in classical statistical mechanics," *Physics Letters A*, vol. 68, no. 5, pp. 421–423, 1978, ISSN: 0375-9601. DOI: https://doi.org/10.1016/0375-9601(78)90615-1. [Online]. Available: https://www.sciencedirect.com/science/article/pii/0375960178906151.

[27] M. E. Fisher, "Renormalization of critical exponents by hidden variables," *Phys. Rev.*, vol. 176, pp. 257–272, 1 Dec. 1968. DOI: 10.1103/PhysRev.176.257. [Online]. Available: https://link.aps.org/doi/10.1103/PhysRev.176.257.

[28] M. Campostrini, M. Hasenbusch, A. Pelissetto, and E. Vicari, "The critical exponents of the superfluid transition in he4," *Physical Review B*, vol. 74, no. 14, Oct. 2006, ISSN: 1550-235X. DOI: 10.1103/physrevb.74.144506. [Online]. Available: http://dx.doi.org/10.1103/PhysRevB.74.144506.

[29] K. Binder, "Critical properties from monte carlo coarse graining and renormalization," *Phys. Rev. Lett.*, vol. 47, pp. 693–696, 9 Aug. 1981. DOI: 10.1103/PhysRevLett.47.693. [Online]. Available: https://link.aps.org/doi/10.1103/PhysRevLett.47.693.

[30] N. Goldenfeld, *Lectures on phase transitions and the renormalization group*. 1992.

[31] S. P. Cockburn and N. P. Proukakis, "The stochastic gross-pitaevskii equation and some applications," *Laser Physics*, vol. 19, no. 4, pp. 558–570, Apr. 2009, ISSN: 1555-6611. DOI: 10.1134/s1054660x09040057. [Online]. Available: http://dx.doi.org/10.1134/S1054660X09040057.

[32] P. C. Hohenberg and B. I. Halperin, "Theory of dynamic critical phenomena," *Rev. Mod. Phys.*, vol. 49, pp. 435–479, 3 Jul. 1977. DOI: 10.1103/RevModPhys.49.435. [Online]. Available: https://link.aps.org/doi/10.1103/RevModPhys.49.435.

[33] R. Toral, "Noise induced transitions vs. noise induced phase transitions," *AIP Conference Proceedings*, vol. 1332, no. 1, pp. 145–154, Mar. 2011, ISSN: 0094-243X. DOI: 10.1063/1.3569493. eprint: https://pubs.aip.org/aip/acp/article-pdf1332/1/145/12109027/145_1_online.pdf. [Online]. Available: https://doi.org/10.1063/1.3569493.

[34] H. B. Callen and T. A. Welton, "Irreversibility and generalized noise," *Phys. Rev.*, vol. 83, pp. 34–40, 1 Jul. 1951. DOI: 10.1103/PhysRev.83.34. [Online]. Available: https://link.aps.org/doi/10.1103/PhysRev.83.34.

[35] W. M. Saslow, "A history of thermodynamics: The missing manual," *Entropy*, vol. 22, no. 1, 2020, ISSN: 1099-4300. DOI: 10.3390/e22010077. [Online]. Available: https://www.mdpi.com/1099-4300/22/1/77.

[36] E. Mendoza, "A sketch for a history of early thermodynamics," *Physics Today*, vol. 14, no. 2, pp. 32–42, Feb. 1961, ISSN: 0031-9228. DOI: 10.1063/1.3057388. eprint: https://pubs.aip.org/physicstoday/article-pdf14/2/32/8256141/32_1_online.pdf. [Online]. Available: https://doi.org/10.1063/1.3057388.

[37] M. Popovic, *Researchers in an entropy wonderland: A review of the entropy concept*, 2017. arXiv: 1711.07326 [physics.chem-ph]. [Online]. Available: https://arxiv.org/abs/1711.07326.

[38] U. Seifert, "Stochastic thermodynamics, fluctuation theorems and molecular machines," *Reports on Progress in Physics*, vol. 75, no. 12, p. 126 001, Nov. 2012. DOI: 10.1088/0034-4885/75/12/126001. [Online]. Available: https://dx.doi.org/10.1088/0034-4885/75/12/126001.

[39] N. Shiraishi, *An Introduction to Stochastic Thermodynamics: From Basic to Advanced* (Fundamental Theories of Physics), 1st ed. Singapore: Springer Singapore, 2023, vol. 212, pp. XIV+443, Published: 08 May 2023, ISBN: 978-981-19-8185-2. DOI: 10.1007/978-981-19-8186-9. [Online]. Available: https://doi.org/10.1007/978-981-19-8186-9.

[40] U. Seifert, "Entropy production along a stochastic trajectory and an integral fluctuation theorem," *Physical Review Letters*, vol. 95, no. 4, Jul. 2005, ISSN: 1079-7114. DOI: 10.1103/physrevlett.95.040602. [Online]. Available: http://dx.doi.org/10.1103/PhysRevLett.95.040602.

[41] D. Zwicker, "Py-pde: A python package for solving partial differential equations," *Journal of Open Source Software*, vol. 5, no. 48, p. 2158, 2020. DOI: 10.21105/joss.02158. [Online]. Available: https://doi.org/10.21105/joss.02158.

[42] P. Virtanen *et al.*, "Scipy 1.0-fundamental algorithms for scientific computing in python," *CoRR*, vol. abs/1907.10121, 2019. arXiv: 1907.10121. [Online]. Available: http://arxiv.org/abs/1907.10121.

[43] A. M. Ferrenberg, J. Xu, and D. P. Landau, "Pushing the limits of monte carlo simulations for the three-dimensional ising model," *Physical Review E*, vol. 97, no. 4, Apr. 2018, ISSN: 2470-0053. DOI: 10.1103/physreve.97.043301. [Online]. Available: http://dx.doi.org/10.1103/PhysRevE.97.043301.

[44] F. Ortega-Zamorano, M. Montemurro, S. Cannas, J. Jerez, and L. Franco, "Fpga hardware acceleration of monte carlo simulations for the ising model," *IEEE Transactions on Parallel and Distributed Systems*, vol. 27, pp. 1–1, Jan. 2015. DOI: 10.1109/TPDS.2015.2505725.

[45] D. Poland, S. Rychkov, and A. Vichi, "The conformal bootstrap: Theory, numerical techniques, and applications," *Reviews of Modern Physics*, vol. 91, no. 1, Jan. 2019, ISSN: 1539-0756. DOI: 10.1103/revmodphys.91.015002. [Online]. Available: http://dx.doi.org/10.1103/RevModPhys.91.015002.

A

Derivation of Free Energy Coefficients

Starting at

$$\mathcal{Z} = \mathcal{N} \int_{-\infty}^{\infty} D\phi \, e^{-\sum_{ij} \phi_i (\beta J_{ij}) \phi_j + \sum_i \ln\left(\cosh\left(\sum_j 2\beta J_{ij}\phi_j\right)\right)} \tag{A.1}$$

we perform a Fourier expansion of the field, $\phi_i = \frac{1}{\sqrt{N}} \sum_{\mathbf{k}} e^{-i\mathbf{k}\cdot\mathbf{r}_i}\phi_{\mathbf{k}}$ and the correlation matrix, $J_{ij} = \frac{1}{N}\sum_{\mathbf{k}} e^{-i\mathbf{k}\cdot(\mathbf{r}_i - \mathbf{r}_j)} J_{\mathbf{k}}$

Expanding the first term of the action gives us

$$\begin{aligned}
\beta \sum_{ij} \phi_i J_{ij} \phi_j &= \beta \sum_{ij} \left(\frac{1}{\sqrt{N}} \sum_{\mathbf{k}} e^{-i\mathbf{k}\cdot\mathbf{r}_i}\phi_{\mathbf{k}}\right)\left(\frac{1}{N}\sum_{\mathbf{l}} e^{-i\mathbf{l}\cdot(\mathbf{r}_i - \mathbf{r}_j)} J_{\mathbf{l}}\right)\left(\frac{1}{\sqrt{N}} \sum_{\mathbf{q}} e^{-i\mathbf{q}\cdot\mathbf{r}_j}\phi_{\mathbf{q}}\right) \\
&= \beta \sum_{\mathbf{klq}} \frac{1}{N}\sum_i e^{-i\mathbf{r}_i\cdot(\mathbf{l}+\mathbf{k})} \frac{1}{N}\sum_j e^{-i\mathbf{r}_j\cdot(\mathbf{q}-\mathbf{l})} \phi_{\mathbf{k}} J_{\mathbf{l}} \phi_{\mathbf{q}} \\
&= \beta \sum_{\mathbf{klq}} \delta_{\mathbf{k},-\mathbf{l}}\delta_{\mathbf{q},\mathbf{l}} \phi_{\mathbf{k}} J_{\mathbf{l}} \phi_{\mathbf{q}} = \beta \sum_{\mathbf{k}} \phi_{\mathbf{k}} J_{-\mathbf{k}} \phi_{-\mathbf{k}} \\
&= \beta \sum_{\mathbf{k}} \phi_{\mathbf{k}} \left(J(0) + \frac{1}{2}\mathbf{k}^2 J''(0)\right) \phi_{-\mathbf{k}} + \mathcal{O}(\mathbf{k}^4),
\end{aligned} \tag{A.2}$$

where we in the last step Taylor expand J in even powers of $\mathbf{k}$, due to it being translationally invariant. For the second term we will start by Taylor expanding $\ln\cosh(...)$

$$\sum_i \ln\cosh\left(\sum_j 2\beta J_{ij}\phi_j\right) = \sum_i \frac{1}{2}\underbrace{\left(\sum_j 2\beta J_{ij}\phi_j\right)^2}_{A} - \frac{1}{12}\sum_i \underbrace{\left(\sum_j 2\beta J_{ij}\phi_j\right)^4}_{B} + \mathcal{O}\left(\phi^6\right). \tag{A.3}$$

By Fourier expanding term A we then get

$$\begin{aligned} A &= 4\beta^2 \left(\sum_j \left(\frac{1}{N} \sum_{\mathbf{k}} e^{-i\mathbf{k}\cdot(\mathbf{r}_i - \mathbf{r}_j)} J_{\mathbf{k}} \right) \left(\frac{1}{\sqrt{N}} \sum_{\mathbf{l}} e^{-i\mathbf{l}\cdot\mathbf{r}_j} \right) \right)^2 \\ &= 4\beta^2 \left(\frac{1}{\sqrt{N}} \sum_{\mathbf{kl}} \frac{1}{N} \sum_j e^{-i\mathbf{r}_j\cdot(\mathbf{l}-\mathbf{k})} J_{\mathbf{k}} \phi_{\mathbf{l}} e^{-i\mathbf{k}\cdot\mathbf{r}_i} \right)^2 = 4\beta^2 \left(\frac{1}{\sqrt{N}} \sum_{\mathbf{kl}} \delta_{\mathbf{k},\mathbf{l}} J_{\mathbf{k}} \phi_{\mathbf{l}} e^{-i\mathbf{k}\cdot\mathbf{r}_i} \right)^2 \\ &= 4\beta^2 \left(\frac{1}{\sqrt{N}} \sum_{\mathbf{k}} J_{\mathbf{k}} \phi_{\mathbf{k}} e^{-i\mathbf{k}\cdot\mathbf{r}_i} \right)^2 = 4\beta^2 \sum_{\mathbf{k}} \phi_{\mathbf{k}} \phi_{-\mathbf{k}} J_{\mathbf{k}}^2 \\ &= 4\beta^2 \sum_{\mathbf{k}} \phi_{\mathbf{k}} \phi_{-\mathbf{k}} \left(J(0)^2 + \mathbf{k}^2 J(0) J''(0) \right) + \mathcal{O}(\mathbf{k}^4). \end{aligned} \tag{A.4}$$

And term B is then given by

$$B = ... = 16\beta^4 \frac{1}{N} \sum_{\mathbf{k}_1\mathbf{k}_2\mathbf{k}_3\mathbf{k}_4} \phi_{\mathbf{k}_1} \phi_{\mathbf{k}_2} \phi_{\mathbf{k}_3} \phi_{\mathbf{k}_4} \delta_{\mathbf{k}_1+\mathbf{k}_2+\mathbf{k}_3+\mathbf{k}_4,0} J(0)^4 \tag{A.5}$$

Collecting all the terms gives us the following momentum-space action:

$$\begin{aligned} S[\phi] = \sum_{\mathbf{k}} \phi_{\mathbf{k}} \phi_{-\mathbf{k}} \left[\beta \left(J(0) + \frac{1}{2}\mathbf{k}^2 J''(0) \right) + 2\beta^2 J(0) \left(J(0) + \mathbf{k}^2 J''(0) \right) \right] \\ + \frac{4}{3}\beta^4 \frac{1}{N} \sum_{\mathbf{k}_1\mathbf{k}_2\mathbf{k}_3\mathbf{k}_4} \phi_{\mathbf{k}_1} \phi_{\mathbf{k}_2} \phi_{\mathbf{k}_3} \phi_{\mathbf{k}_4} \delta_{\mathbf{k}_1+\mathbf{k}_2+\mathbf{k}_3+\mathbf{k}_4,0} J(0)^4. \end{aligned} \tag{A.6}$$

If we now transform back to position-space and take the continuum limit we get

$$S[\phi] = \int d^d x \, c_1 \left(\nabla\phi \right)^2 + c_2 \phi^2 + c_3 \phi^4 \tag{A.7}$$

where $c_1 = \frac{\beta}{2} J''(0) \left(1 - 4\beta J(0)\right)$, $c_2 = \beta J(0) \left(1 - 2\beta J(0)\right)$ and $c_3 = \frac{4\beta^4}{3} J(0)^4$.

B

Full Comparison of Analytical and Numerical Results

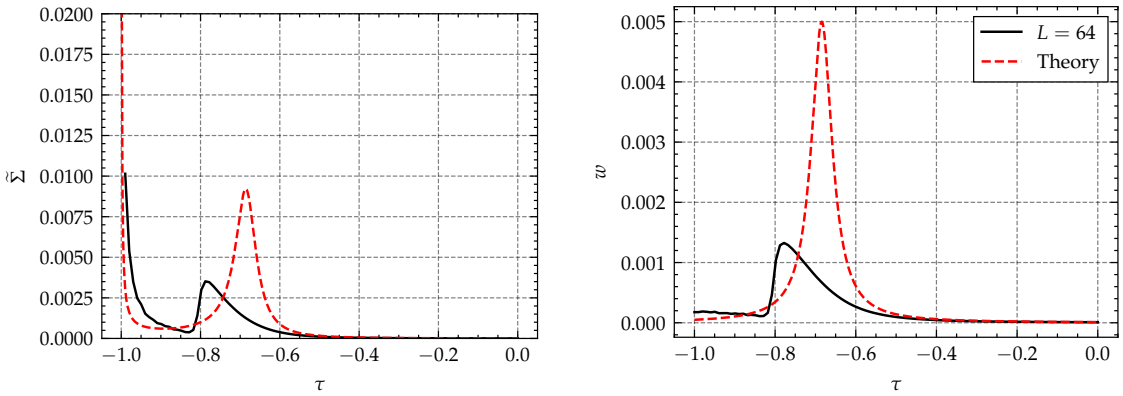

(a) Numerical simulation and analytical calculation of entropy production plotted against the control parameter τ.

(b) Numerical simulation and analytical calculation of dissipated heat plotted against the control parameter τ.

Figure B.1: Comparison between analytical and numerical results for a 2D, $L = 64$ field with a driving frequency $\omega = 0.01\pi$.

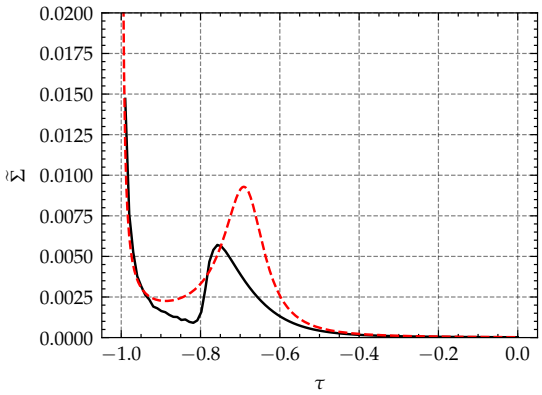

(a) Numerical simulation and analytical calculation of entropy production plotted against the control parameter τ.

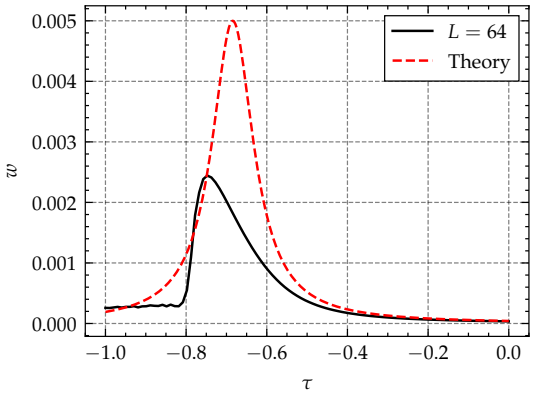

(b) Numerical simulation and analytical calculation of dissipated heat plotted against the control parameter τ.

Figure B.2: Comparison between analytical and numerical results for a 2D, $L = 64$ field with a driving frequency $\omega = 0.02\pi$.

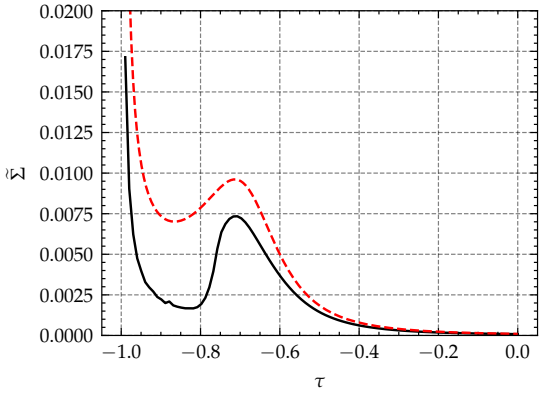

(a) Numerical simulation and analytical calculation of entropy production plotted against the control parameter τ.

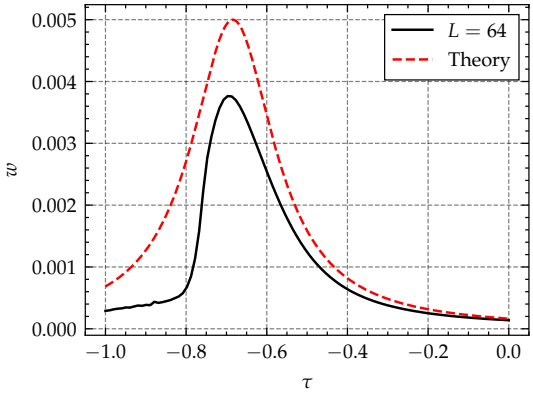

(b) Numerical simulation and analytical calculation of dissipated heat plotted against the control parameter τ

Figure B.3: Comparison between analytical and numerical results for a 2D, $L = 64$ field with a driving frequency and amplitude of $\omega = 0.04\pi$ and $h_0 = 0.1$.

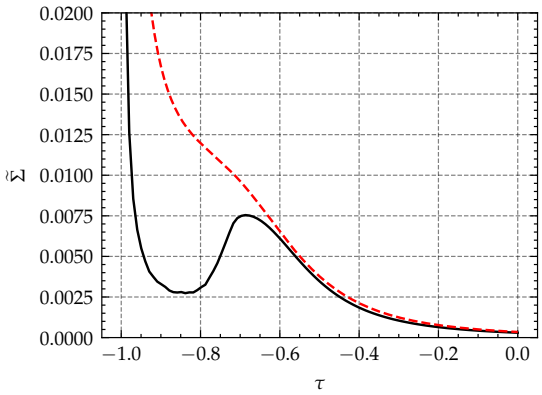

(a) Numerical simulation and analytical calculation of entropy production plotted against the control parameter τ.

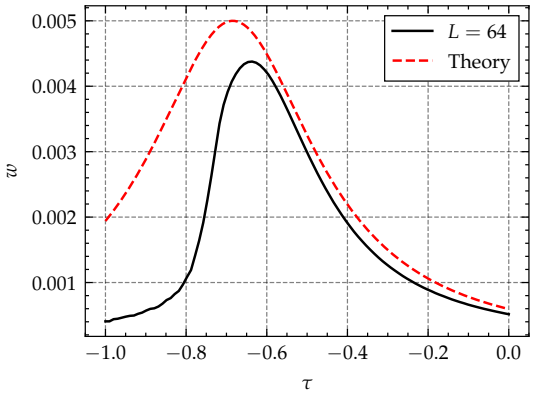

(b) Numerical simulation and analytical calculation of dissipated heat plotted against the control parameter τ.

Figure B.4: Comparison between analytical and numerical results for a 2D, $L = 64$ field with a driving frequency and amplitude of $\omega = 0.08\pi$ and $h_0 = 0.1$.

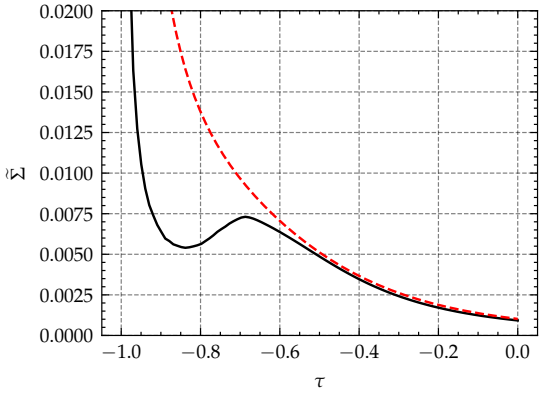

(a) Numerical simulation and analytical calculation of entropy production plotted against the control parameter τ.

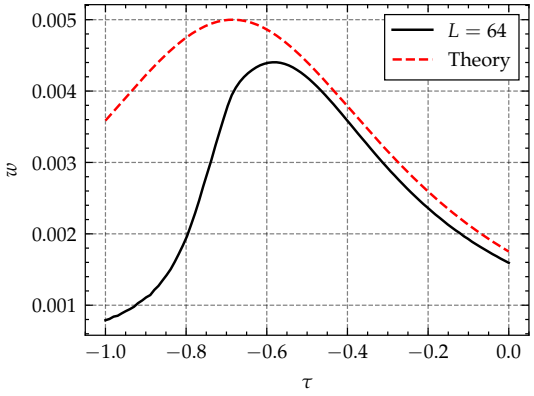

(b) Numerical simulation and analytical calculation of dissipated heat plotted against the control parameter τ.

Figure B.5: Comparison between analytical and numerical results for a 2D, $L = 64$ field with a driving frequency and amplitude of $\omega = 0.16\pi$ and $h_0 = 0.1$.

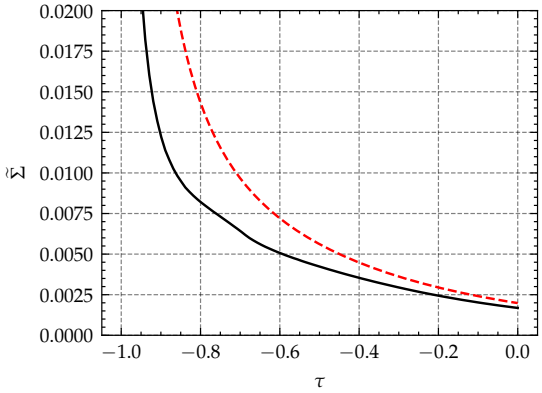

(a) Numerical simulation and analytical calculation of entropy production plotted against the control parameter τ.

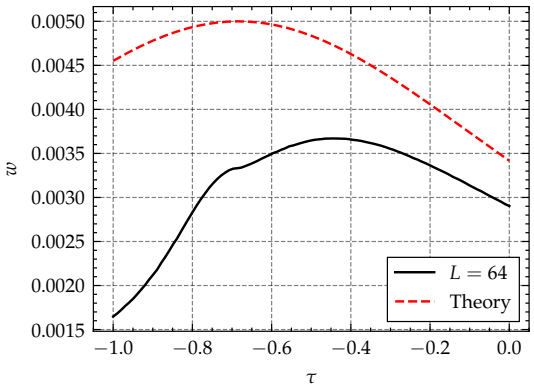

(b) Numerical simulation and analytical calculation of dissipated heat plotted against the control parameter τ.

Figure B.6: Comparison between analytical and numerical results for a 2D, $L = 64$ field with a driving frequency $\omega = 0.32\pi$.

DEPARTMENT OF PHYSICS
CHALMERS UNIVERSITY OF TECHNOLOGY
Gothenburg, Sweden
www.chalmers.se

CHALMERS
UNIVERSITY OF TECHNOLOGY